Immunotherapy targeting the C-terminal domain of TDP-43 decreases neuropathology and confers neuroprotection in mouse models of ALS/FTD

Article *in* Neurobiology of Disease · February 2023

DOI: 10.1016/j.nbd.2023.106050

CITATIONS
0

READS
29

26 authors, including:

Tariq Afroz
AC Immune SA
13 PUBLICATIONS **652** CITATIONS
SEE PROFILE

Mickael Audrain
AC Immune SA
91 PUBLICATIONS **970** CITATIONS
SEE PROFILE

Christopher Dumayne
AC Immune SA
10 PUBLICATIONS **86** CITATIONS
SEE PROFILE

Anne-Laure Egesipe
Nestlé Institute of Health Sciences S.A.
29 PUBLICATIONS **208** CITATIONS
SEE PROFILE

Neurobiology of Disease 179 (2023) 106050

Contents lists available at ScienceDirect

Neurobiology of Disease

journal homepage: www.elsevier.com/locate/ynbdi

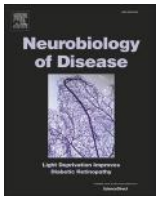

Immunotherapy targeting the C-terminal domain of TDP-43 decreases neuropathology and confers neuroprotection in mouse models of ALS/FTD

Tariq Afroz [a,*], Elodie Chevalier [a,1], Mickael Audrain [a,1], Christopher Dumayne [a], Tamar Ziehm [a], Roger Moser [a], Anne-Laure Egesipe [a], Lorène Mottier [a], Monisha Ratnam [a], Manuela Neumann [b,c], Daniel Havas [d], Romain Ollier [a], Kasia Piorkowska [a], Mayank Chauhan [a], Alberto B. Silva [a], Samjhana Thapa [a], Jan Stöhr [a,2], Andrej Bavdek [a], Valerie Eligert [a], Oskar Adolfsson [a], Peter T. Nelson [e], Sílvia Porta [f], Virginia M.-Y. Lee [f], Andrea Pfeifer [a], Marie Kosco-Vilbois [a], Tamara Seredenina [a,*]

[a] AC Immune SA, Lausanne, Switzerland
[b] Department of Neuropathology, University of Tübingen, Tübingen, Germany
[c] DZNE, German Center for Neurodegenerative Diseases, Tübingen, Germany
[d] Psychogenics Inc., Paramus, NJ, USA
[e] University of Kentucky, Lexington, KY, USA
[f] Center for Neurodegenerative Disease Research (CNDR), Institute on Aging, Department of Pathology and Laboratory Medicine, Perelman School of Medicine, University of Pennsylvania, Philadelphia, PA 19104, USA

ARTICLE INFO

Keywords:
TDP-43
Immunotherapy
Frontotemporal dementia (FTD)
Amyotrophic lateral sclerosis (ALS)
Microglia

ABSTRACT

Effective therapies are urgently needed to safely target TDP-43 pathology as it is closely associated with the onset and development of devastating diseases such as frontotemporal lobar degeneration with TDP-43 pathology (FTLD-TDP) and amyotrophic lateral sclerosis (ALS). In addition, TDP-43 pathology is present as a co-pathology in other neurodegenerative diseases such as Alzheimer's disease and Parkinson's disease. Our approach is to develop a TDP-43-specific immunotherapy that exploits Fc gamma-mediated removal mechanisms to limit neuronal damage while maintaining physiological TDP-43 function. Thus, using both *in vitro* mechanistic studies in conjunction with the rNLS8 and CamKIIa inoculation mouse models of TDP-43 proteinopathy, we identified the key targeting domain in TDP-43 to accomplish these therapeutic objectives. Targeting the C-terminal domain of TDP-43 but not the RNA recognition motifs (RRM) reduces TDP-43 pathology and avoids neuronal loss *in vivo*. We demonstrate that this rescue is dependent on Fc receptor-mediated immune complex uptake by microglia. Furthermore, monoclonal antibody (mAb) treatment enhances phagocytic capacity of ALS patient-derived microglia, providing a mechanism to restore the compromised phagocytic function in ALS and FTD patients. Importantly, these beneficial effects are achieved while preserving physiological TDP-43 activity. Our findings demonstrate that a mAb targeting the C-terminal domain of TDP-43 limits pathology and neurotoxicity, enabling clearance of misfolded TDP-43 through microglia engagement, and supporting the clinical strategy to target TDP-43 by immunotherapy.

Significance statement: TDP-43 pathology is associated with various devastating neurodegenerative disorders with high unmet medical needs such as frontotemporal dementia (FTD), amyotrophic lateral sclerosis (ALS) and Alzheimer's disease. Thus, safely and effectively targeting pathological TDP-43 represents a key paradigm for biotechnical research as currently there is little in clinical development. After years of research, we have determined that targeting the C-terminal domain of TDP-43 rescues multiple patho-mechanisms involved in disease progression in two animal models of FTD/ALS. In parallel, importantly, our studies establish that this approach does not alter the physiological functions of this ubiquitously expressed and indispensable protein.

* Corresponding authors at: AC Immune SA, EPFL Innovation Park Building B, 1015 Lausanne, Switzerland.
E-mail addresses: tariq.afroz@acimmune.com (T. Afroz), tamara.seredenina@acimmune.com (T. Seredenina).
[1] These authors equally contributed to the manuscript.
[2] Current affiliation: AbbVie, Neuroscience Discovery, Cambridge, MA, USA.

https://doi.org/10.1016/j.nbd.2023.106050
Received 20 December 2022; Received in revised form 10 February 2023; Accepted 16 February 2023
Available online 20 February 2023

Together, our findings substantially contribute to the understanding of TDP-43 pathobiology and support the prioritization for clinical testing of immunotherapy approaches targeting TDP-43.

1. Introduction

Misfolded aggregates of transactive response DNA binding protein 43 (TDP-43) are a hallmark of multiple neurodegenerative pathologies including amyotrophic lateral sclerosis and frontotemporal dementia (ALS-FTD) disease spectrum (Neumann et al., 2006; Arai et al., 2006) and limbic-predominant age-related TDP-43 encephalopathy (LATE) (Nelson et al., 2019). Moreover, these aggregated forms have been identified as co-pathologies in Alzheimer's disease (AD), Parkinson's disease (PD) and chronic traumatic encephalopathy (CTE) as well as in rare conditions such as inclusion body myositis (IBM) (Karanth et al., 2020; McKee et al., 2010; Salajegheh et al., 2009; Chornenkyy et al., 2019). Accumulating evidence shows a correlation of clinical progression in ALS and FTLD-TDP with spatiotemporal distribution of pathological TDP-43 species in neuroanatomically connected brain regions suggesting that cell-to-cell propagation of TDP-43 pathology contributes to disease progression (Brettschneider et al., 2013; Kawakami et al., 2019). Indeed, various subtypes for FTLD-TDP (*i.e.*, A, B, C, D and E) have been defined based on the morphology and regional localization of intracellular TDP-43 aggregates in neuronal and glial cells (Mackenzie et al., 2011; Tsuji et al., 2012; Lee et al., 2017; Neumann et al., 2021). Cell-to-cell transmission has been recapitulated using self-templating TDP-43 that leads to pathological aggregate formation and disease progression (Porta et al., 2018; Feiler et al., 2015; Nonaka et al., 2013), corroborating the hypothesis of TDP-43 spreading. Furthermore, using recently developed techniques, Scialo et al., 2020 (Scialo et al., 2020) have demonstrated that seeding-competent species exist in the CSF of patients with FTD and ALS. Therefore, multiple mechanisms contribute to spreading of TDP-43 pathology including transmission across synaptic terminals, exosomes and release of misfolded TDP-43 from dying neurons. Thus, preventing the progression of TDP-43 neuropathology in the central nervous system (CNS) through enhanced clearance of extracellular TDP-43 by immune complex-mediated engagement of microglia and the resulting decrease of templated aggregation is an attractive strategy for therapeutic intervention.

The exact composition of the extracellular species responsible for prion-like transmission remains elusive in part due to the lack of specific and sensitive reagents for detection (Feneberg et al., 2018). While TDP-43 is an important nuclear RNA/DNA-binding protein involved in the regulation of RNA processing, TDP-43 pathology commences as reduced TDP-43 levels in the nuclei and aberrant accumulation with aggregate formation predominantly in the cytoplasm. Furthermore, post-translational modifications are induced including ubiquitination, acetylation, sumoylation, phosphorylation at multiple sites and fragmentation (*i.e.*, formation of aggregation-prone C-terminal fragments) (Neumann et al., 2009; Cohen et al., 2015; Maurel et al., 2020; Seyfried et al., 2010; Buratti, 2018). Indeed, C-terminal fragments harboring the amyloid core are enriched in FTLD-TDP patients (Arai et al., 2006; Arseni et al., 2021), acting to further induce the formation of aggregated TDP-43. Moreover, TDP-43 autoantibodies binding to the C-terminal region are observed in the sera of ALS patients, demonstrating that the C-terminal epitope is exposed in the extracellular environment, activating the immune system (Simula et al., 2021; Conti et al., 2021; Nielsen et al., 2021). Taken together, these findings support a classical immunotherapy approach to safely provide therapeutic benefit by reducing extracellular pathological TDP-43 transmission, enhancing clearance of pathology by microglia, preventing further neurotoxicity exerted by pathological TDP-43 (Laferriere et al., 2019; Hergesheimer et al., 2019) while maintaining endogenous TDP-43 function.

Here, we report the investigations undertaken to study targeting extracellular TDP-43 with antibodies, validating the therapeutic approach. From a panel of antibodies generated using full length TDP-43 as the immunogen, two mAbs, ACI-5891 and ACI-5886, were selected for further characterization based on distinct epitope coverage yet similar target binding data. Assessed side by side, ACI-5891, the mAb targeting the C-terminal domain of TDP-43, significantly reduced seeding *in vitro* and decreased the levels of aggregated and phosphorylated TDP-43 in the rNLS8 mouse model. In contrast, ACI 5886, targeting the region in RNA binding domain, did not differ from the controls. ACI-5891 was then progressed into a second model of human disease, the CamKIIa-hTDP-43NLSm inoculation model, in which decreased pathology was confirmed as well as neuroprotection observed. The effect of ACI-5891 was driven by microglia and Fc-mediated immune complex clearance as alteration of morphology and a decrease in efficacy was observed when using the Fc effector-reduced version of ACI-5891. Together, these results of inducing neuroprotection with reduction of TDP-43 neuropathology validate the immunotherapy approach as well as validate ACI-5891 as a potential therapeutic antibody.

2. Results

2.1. Binding characteristics and specificity of two mAbs to distinct epitopes in TDP-43

Using the SupraAntigen® platform to obtain a panel of anti-TDP-43 mAbs, a liposome-based vaccine was created (Muhs et al., 2007) by conjugation with the target of interest, recombinant full length TDP-43 (Fig. S1A). Evaluating binding characteristics, epitopes and target engagement on patient brain sections, two mAbs were selected. As shown by ELISA on peptides covering the sequence of TDP-43, ACI-5891 binds in the C-terminal region (Fig. S1B) which is important for aggregation (Guenther et al., 2018), whereas, ACI-5886, binds in the RNA binding domain (Fig. S1B). The two mAbs bind to TDP-43 with high affinity as demonstrated by an ELISA from which an EC_{50} of 0.13 and 0.15 nM was obtained for ACI-5891 and ACI-5886, respectively, (Fig. 1A). The binding affinity, K_D, for the full-length human recombinant aggregated TDP-43 is sub-nanomolar for both mAbs, 0.182 and 0.691 nM, respectively (Fig. 1B, upper panels). To obtain monovalent binding affinity, Fab fragments were generated and a K_D of 2.8 and 21.8 nM for ACI-5891 and ACI-5886, respectively, observed (Fig. 1B, lower panels) explaining the slightly lower avidity of the latter to TDP-43 as compared with ACI-5891. The target specificity of ACI-5891 and ACI-5886 was further confirmed by the reduction of the signal on an immunoblot following the knock-down of TDP-43 using specific siRNA in the HEK-293 cell line (Fig. 1C). TDP-43 knockdown was further confirmed using a commercial TDP-43 antibody that detected the reduction of TDP-43 signal, similar to ACI-5891 and ACI-5886 (Fig. 1C).

2.2. Characterization of target engagement to disease and physiological forms of TDP-43

Postmortem tissues, obtained from FTLD-TDP brain and ALS spinal cord cases, illustrated the characteristics of the TDP-43 species labeled and confirmed target engagement (Fig. 1D). Immunohistochemistry (IHC) studies revealed the expected nuclear labeling corresponding to physiological TDP-43 with both ACI-5891 and ACI-5886. In addition, labeling of multiple forms of pathological TDP-43 were observed with both antibodies. In sections from FTLD-TDP type A, compact neuronal cytoplasmic inclusions (NCI), short dystrophic neurites (DN) and lentiform neuronal intranuclear inclusions (NII) could be identified. In sections from FTLD-TDP type B and ALS, the expected diffuse granular NCI and thread/dots were delineated as well as long thick DN in sections

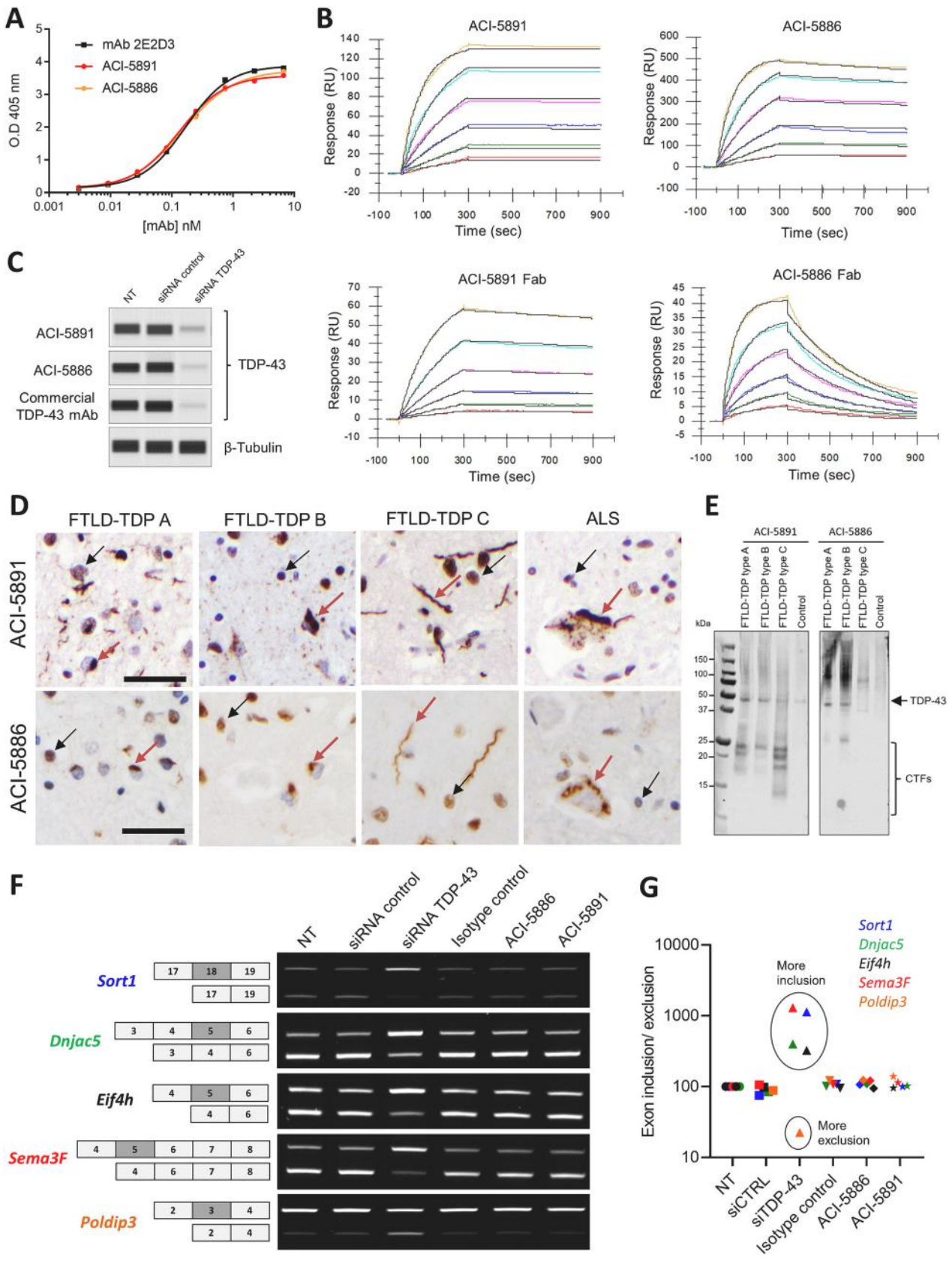

(caption on next page)

Fig. 1. Monoclonal antibodies bind with high affinity to TDP-43, show target engagement on ALS and FTLD-TDP tissues and do not perturb TDP-43 function. (A) Binding of ACI-5891 (red), ACI-5886 (orange), and 2E2-D3 commercial TDP-43 antibody (black) to human recombinant TDP-43 by ELISA. Optical density (OD) at 405 nm on y-axis is shown for different antibody concentrations on the x-axis. (B) Top part: binding of ACI-5891 (left panel) and ACI-5886 (right panel) to immobilized recombinant aggregated TDP-43 assessed by SPR. Bottom part: binding of ACI-5891 Fab (left panel) and ACI-5886 Fab (right panel) to immobilized full-length TDP-43 assessed by SPR. Response units (Y axis, in RU) are plotted against time (X axis, in *sec*) for the following concentrations: 3.2 nM (red), 6.3 nM (green), 12.5 nM (blue), 25 nM (purple), 50 nM (light blue) and 100 nM (yellow). The graphs present an overlay of sensorgrams (in colour) and kinetic fit (in black). (C) Immunodetection following capillary electrophoresis of total cell lysates with TDP-43 antibodies (ACI-5891, ACI-5886 and a commercial mAb) and β-tubulin (lower panel), showing specificity of TDP-43 mAbs resulting in a reduction of signal upon siRNA mediated downregulation of TDP-43 in HEK-293 cells. (D) ACI-5891 and ACI-5886 labels pathological TDP-43 inclusions (red arrows) as well as nuclear physiological TDP-43 (black arrows) in postmortem human tissue sections from FTLD-TDP type A, B or C cases (temporal cortex) and in spinal cord from an ALS case. Scale bar 50 μm. (E) Immunoblot using ACI-5891 (left) and ACI-5886 (right) on sarkosyl-insoluble extracts prepared from brains (frontal cortex) of patients with FTLD-TDP type A, B or C pathology or a control donor. Four micrograms (μg) of total protein in sarkosyl-insoluble extracts were loaded for each lane. Molecular weight marker is shown on the left (kDa). Arrow indicates the expected molecular weight for TDP-43. Brace indicate expected molecular weight for TDP-43 C-terminal fragments. (F) Semi-quantitative RT-PCR analysis of alternative splicing for selected TDP-43 targets (*Sort1*, *Dnjac5*, *Eif4h*, *Sema3F* and *Poldip3*) in C17.2 cells treated with siRNA control, siRNA TDP-43, IgG2a isotype control, ACI-5886 and ACI-5891. Left panel depicts alternatively spliced exons (gray) flanked by their constitutive exons (white). Right panel shows representative polyacrylamide gel images of semi-quantitative RT-PCR products for all conditions. (G) Quantification of splicing changes plotted as the ratio of exon inclusion/exclusion (y-axis) against different treatment conditions (x-axis) averaged from two biological replicates and normalized to the ratio obtained for not treated (NT) cells that is arbitrarily set to 100. Full gels corresponding to Fig. 1C and Fig. 1F and shown in Fig. S8A and Fig. S8B, respectively. (For interpretation of the references to colour in this figure legend, the reader is referred to the web version of this article.)

from FTLD-TDP type C (Fig. 1D).

TDP-43 has several disease-associated phosphorylation sites (Neumann et al., 2009). To confirm binding when the protein is phosphorylated in the region of its epitope, the labeling of ACI-5891 was combined with that of an antibody (1D3), a mAb directed to a phosphorylated form of TDP-43, *i.e.*, pS409/410. ACI-5891 labeling overlapped with the pathological TDP-43 inclusions identified by the mAb, 1D3 (Fig. S1C), further exemplifying its capacity to bind disease-associated forms of the protein.

ACI-5891 binding was also assessed on postmortem brain sections obtained from the hippocampus of patients diagnosed by pathological evaluation with LATE. In these sections, ACI-5891 labeled neuronal cytoplasmic inclusions that colocalized with labeling of phosphorylated TDP-43 aggregates (Fig. S1D). Furthermore, in sections prepared postmortem from AD and PD patients, ACI-5891 labeled nuclear TDP-43 as expected, but did not label senile plaques, neurofibrillary tangles nor Lewy pathology (Fig. S1E) further confirming specificity for TDP-43.

To further characterize the TDP-43 species bound by these two mAbs, binding of ACI-5891 and ACI-5886 to sarkosyl-insoluble brain extracts containing aggregated TDP-43 isolated from patients with FTLD-TDP type A, B or C pathology was assessed by western blotting (Fig. 1E). In addition to full-length TDP-43, ACI-5891 detected C-terminal fragments of TDP-43 with molecular weights below 25 kDa. ACI-5886 also detected full-length TDP-43 in the brain homogenate derived from the same patient brains. Interestingly, ACI-5886 detected fewer truncated fragments of TDP-43 as compared to ACI-5891, in line with its epitope being in the RRM domain upstream of the majority of reported cleavage sites (Berning and Walker, 2019) (Fig. 1E). With both mAbs, high-molecular weight TDP-43-positive species were detected representing aggregated and ubiquitinated TDP-43 (Neumann, 2009). Only trace amounts of TDP-43 were detected in the brain extracts from control cases which do not contain sarkosyl-insoluble TDP-43 (Fig. 1E).

As ACI-5891 and ACI-5886 bind both physiological as well as various pathological forms of TDP-43, evaluation of physiological function of TDP-43 was performed to rule out potential undesired effects of mAb treatment. No cellular labeling was observed following incubation of live (*i.e.*, unfixed) neural progenitor cells, C17.2, indicating that the mAbs are not taken up by the cell (Fig. S1F). Furthermore, the incubation with the mAbs did not alter the cellular levels of TDP-43 protein (Fig. S1G-H). Finally, we confirmed that treatment with ACI-5891 or ACI-5886 did not alter the generation of relevant splicing variants (Fig. 1F-G). In contrast, as a control, reduction of TDP-43 levels using a TDP-43-specific siRNA triggered mis-splicing of the following RNA targets, *Sort1*, *Dnajc5*, *Poldip3*, *Eif4h* and *Sema3F* (Fig. 1F-G).

2.3. Targeting C-terminal domain inhibits TDP-43 de novo aggregation in vitro

Next, ACI-5891 and ACI-5886 were characterized in an *in vitro* aggregation assay recapitulating the initial events in the formation of TDP-43 aggregates (Wang et al., 2018). The two mAbs showed different functional efficacy in inhibition of aggregation (Fig. 2A). ACI-5891 completely inhibited TDP-43 aggregation at a TDP-43-to-mAb equimolar ratio and the curves were indistinguishable from conditions without aggregation induction (*i.e.*, without TEV protease cleavage) (Fig. 2A-B). In contrast, in the presence of ACI-5886, the aggregation kinetics were indistinguishable from the results with the isotype control antibody demonstrating that ACI-5886 did not inhibit or slow down TDP-43 aggregation in this assay. These results were confirmed by sedimentation and quantification of aggregated TDP-43 using an immunodetection assay (Fig. S2A-B).

For ACI-5891, a concentration-dependent inhibition of TDP-43 aggregation resulted in an IC_{50} of 117.5 nM (Fig. 2C-D). As a control in these experiments, TDP-43-MBP cleavage by TEV protease required for the induction of TDP-43 aggregation was not affected by the presence of antibodies (Fig. S2C).

2.4. Targeting C-terminal domain inhibits TDP-43 templated aggregation in vitro

To evaluate the effect on templated aggregation *in vitro*, immunodepletion experiments were performed with aggregated and phosphorylated TDP-43 enriched from FTLD-TDP brain extracts. The immunodepleted fractions demonstrated substantial TDP-43 depletion by the C-terminal binder, ACI-5891, as compared with the isotype control but only partial depletion by the RRM binder, ACI-5886 (Fig. 3A). For quantitative analyses, the signals obtained for total TDP-43 or C-terminal fragments of TDP-43 (*i.e.* 25 kDa, CTF) were normalized to the corresponding signal in the input. ACI-5891 significantly decreased the levels of both full-length TDP-43 (Fig. 3B) and CTFs (Fig. 3C) as compared with isotype control. Even though a trend of reduction of C-terminal fragment was observed by ACI-5886, it was not statistically significant. Since the immunodepletion was performed in a native buffer, a fraction of C-terminal fragment potentially co-aggregated with full-length TDP-43 and resulted in co-immunodepletion by ACI-5886 resulting in the corresponding reduction of signal.

The TDP-43 immunodepleted brain extracts were subsequently tested for their ability to induce templated aggregation in iGFP-NLSm QBI-293 cells, a doxycycline-inducible cell line expressing GFP-tagged cytoplasmic TDP-43 protein (Porta et al., 2018) (Fig. S2D). An equal volume of immunodepleted samples were transduced into the cells and

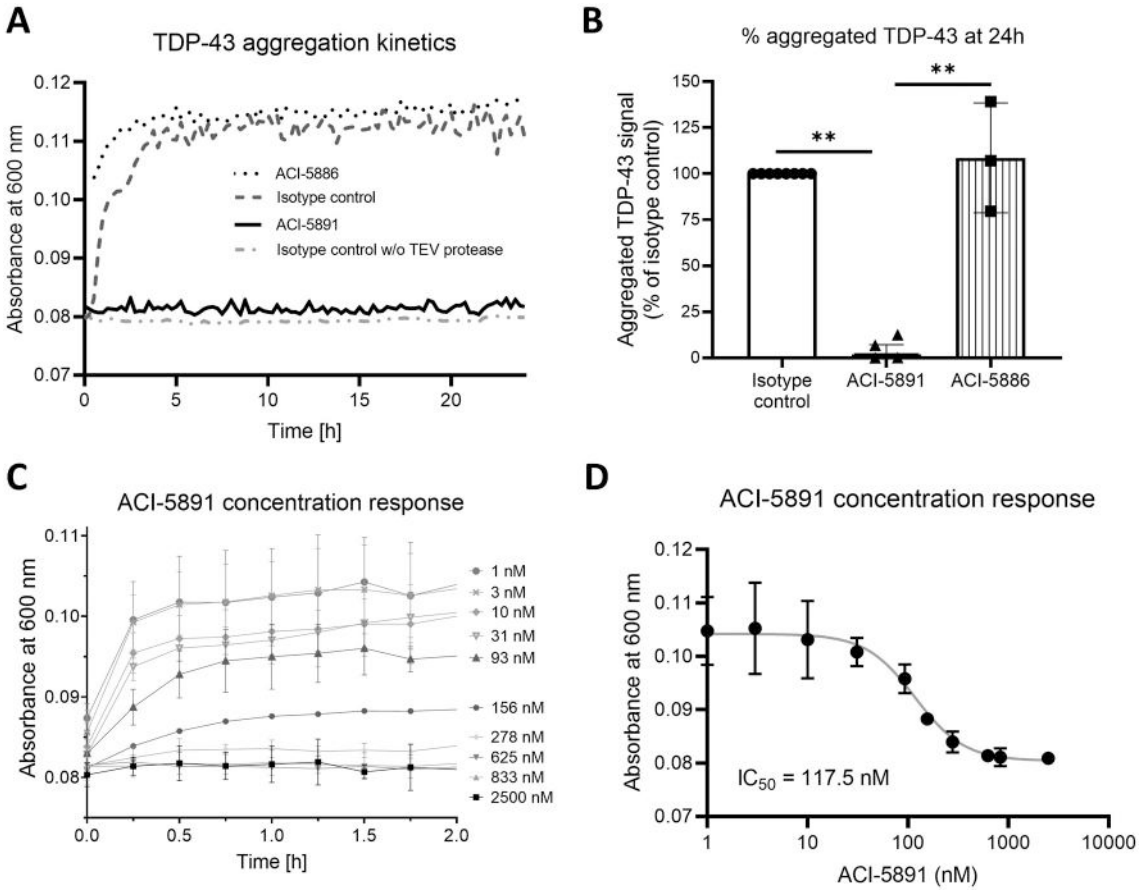

Fig. 2. ACI-5891 inhibits TDP-43 aggregation *in vitro* in a dose-dependent manner.
(A) TDP-43 *de novo* aggregation upon cleavage of MBP-tag was analyzed in the absence or presence of mAbs. Representative aggregation kinetics in the presence of 2.5 μM ACI-5891, ACI-5886 or isotype control equimolar to TDP-43 concentration are shown. Condition without TEV protease shows baseline aggregation. Inhibition of aggregation in the presence of mAbs measured by absorbance (y-axis). (B) For quantification, data in the presence of mAbs for the 24 h time-point were normalized to the isotype control and presented as aggregated TDP-43 signal measured by absorbance. Data shown as mean ± standard deviation (SD) and a Kruskal-Wallis test followed by a Dunn's test for multiple comparisons was used (**$p < 0.01$). (C) For ACI-5891, response curves at different mAb concentrations shown as a mean value of absorbance measured up to 2 h. Data shown as mean ± SD. (D) A concentration response curve was generated with the mean absorbance values measured at 1.5 h for each concentration tested in (C). Data shown as mean ± SD.

seeding activity was analyzed by quantification of the area occupied by *de novo* phosphorylated TDP-43 aggregates (pS409/410 mAb signal colocalizing with TDP-43-GFP fluorescence) (Fig. 3D-E). Both qualitatively (Fig. 3D) and quantitatively (Fig. 3E), ACI-5891 immunodepleted extracts significantly reduced the level of pTDP-43 as compared with the extracts immunodepleted with either isotype control or ACI-5886 (Fig. 3E).

2.5. The C-terminal pan specific mAb, ACI-5891, mitigates TDP-43 pathology in rNLS8 mouse model of TDP-43 proteinopathy

As the *in vitro* assays involving *de novo* and templated aggregation demonstrated a stronger capacity of the C-terminal binding mAb to alter pathological TDP-43 aggregation, the same two mAbs were assessed side by side in the inducible NEFH-tTA x hTDP-43ΔNLS (rNLS8) double transgenic mouse model. These animals were established to study TDP-43 related pathology by expressing the human TDP-43 with a mutation in the nuclear localization signal (hTDP-43 ΔNLS) that also alters the endogenous function of the protein within all neurons (Walker et al., 2015). Target engagement was confirmed using brain sections and homogenates with both mAbs demonstrating binding to RIPA-soluble and RIPA-insoluble fractions (Fig. S3A-B). A single-dose pharmacokinetic study was performed in wild type mice to establish a suitable dosing schedule (*i.e.*, a half-life of 7 days for ACI-5886 and 15 days for ACI-5891, Fig. 4A). Of note, no clinical signs were observed over 28 days in this study. Next, the rNLS8 mice were dosed i.p. weekly for 5 weeks with either ACI-5891, ACI-5886 or the vehicle control (Fig. 4B). The dosing started simultaneously with doxycycline withdrawal, *i.e.*, at the time of inducing hTDP-43 ΔNLS expression. For ACI-5891 and ACI-5886, the average plasma concentrations assessed at the end of the study were 940 μg/mL (6.2 μM) and 493 μg/mL (3.2 μM), respectively (Fig. S3C). Although the terminal plasma concentration of ACI-5886 was lower than that of ACI-5891, their predicted levels in the brain were still well above their respective K_D for TDP-43 binding (0.691 nM for ACI-5886 and 0.182 nM for ACI-5891) assuming 0.1% brain penetration from the plasma as reported for other mAbs with systemic administration (Kouhi et al., 2021).

Phosphorylated TDP-43 inclusions were observed in mice 5 weeks post transgene induction (Fig. 4C). ACI-5891 treatment led to a significant reduction in the density of pTDP-43-positive inclusions in the cerebral cortex compared to ACI-5886 or vehicle-treated mice (Fig. 4D, Fig. S3D) and a similar trend was observed for the immunoreactive area (Fig. S3E) and for striatum (Fig. S3F). These findings were confirmed using biochemical assay that showed reduction in the pTDP-43 levels (Fig. 4E) and in aggregated TDP-43 levels (Fig. 4F) in the RIPA-insoluble fractions of ACI-5891 but not ACI-5886 treated mice as compared to vehicle. Consistent with the cell-based assay (Fig. S1G-H), no significant changes in soluble TDP-43 protein levels were detected after ACI-5891

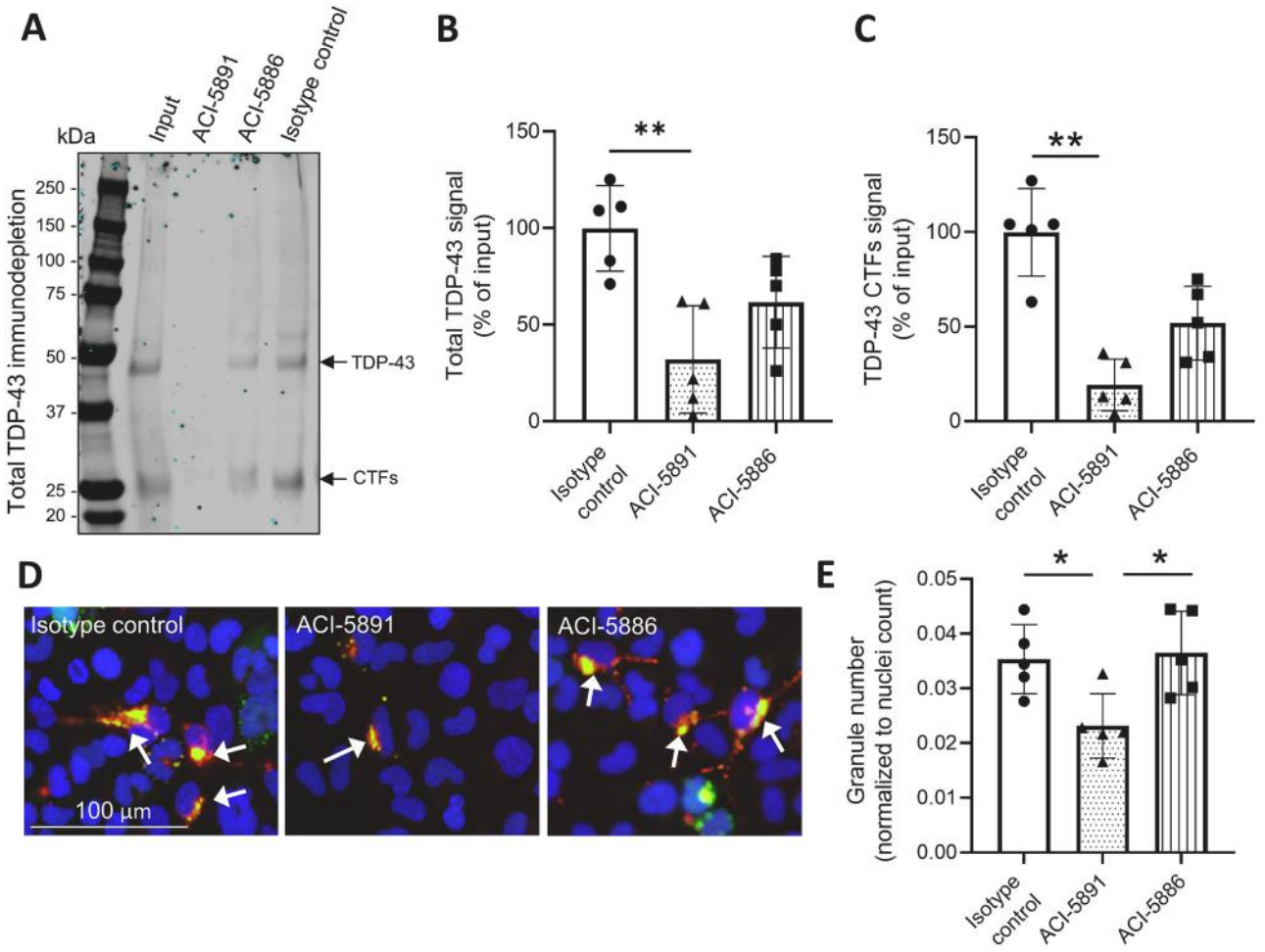

Fig. 3. ACI-5891 inhibits seeded aggregation induced by FTLD-TDP brain derived extracts.
(A) Representative image of TDP-43 immunoblots from FTLD-TDP brain-derived extracts following immunodepletion by either ACI-5891, ACI-5886 or isotype control. Detection was performed using ACI-5891 antibody. (B-C) Quantification of either full-length TDP-43 (B) or C-terminal fragments (C) immunodepletion using data from western blot (A). Data plotted for isotype control (open bars, solid circles), ACI-5891 (dotted bars, solid triangles) and ACI-5886 (striped bar, solid squares) are normalized to input. (D) Immunofluorescence images representative of the effect of mAbs on TDP-43 templated aggregation in the cell model. Cell nuclei were labeled with DAPI (blue) and pTDP-43 (red) and GFP-TDP-43NLSm (green, intrinsic GFP fluorescence). Colocalization between GFP-TDP-43NLSm and pTDP-43 shown in yellow (white arrows). Scale bar = 100 µm. (E) Area of pTDP-43-positive aggregates co-localized with TDP-43-GFP signal in different conditions following immunodepletion with either isotype control mAb, ACI-5891 or ACI-5886 are plotted on y-axis. A Kruskal-Wallis test followed by a Dunn's multiple comparisons test was used for B and C and a one-way ANOVA followed by a Tukey post-hoc test for multiple comparison was used for E. $*p < 0.05$; $**p < 0.01$. Data is shown as mean ± SD. Each point represents a biological (B-C) or technical replicate (E). Experiment described in (E) was independently replicated. (For interpretation of the references to colour in this figure legend, the reader is referred to the web version of this article.)

and ACI-5886 treatment compared with vehicle control (Fig. S3G-H, Fig. 4G). Additionally, mAb treatments did not influence the total number of NeuN-positive neurons in cerebral cortex in this model as expected (Fig. S3I).

Evaluation of body weight and motor function demonstrated a progressive decline in all animals (Fig. S4A-C) following transgene expression prior to the appearance of TDP-43 aggregates (Walker et al., 2015). As mAbs do not affect the transgene expression, no effect of mAbs treatment on body weight, tremor and clasping was observed (Fig. S4A-C).

As a reduction in pTDP-43 but not total TDP-43 levels was observed with ACI-5891, a mAb that is not spontaneously taken up by neurons (Fig. S1F), we hypothesized that extracellular, mainly pathological TDP-43 released in this model was cleared by activated microglia *via* an Fcγ receptor-mediated phagocytosis. Since the phagocytic marker CD68 did not change significantly in the rNLS8 model during disease progression (Spiller et al., 2018), a pan-microglial marker Iba1 was used to evaluate microglial activation. A highly significant increase in Iba1 labeling was observed in the vehicle treated group at 5 weeks post transgene induction (Fig. S4D-E). mAb treatment did not further exacerbate the observed microgliosis and the microglial density remained unchanged (Fig. S4F-G). However, microglial morphology evaluation showed a significant increase in the mean cell size of large ramified microglia, indicative of increased phagocytic activity, in ACI-5891 treated mice as compared to vehicle (Fig. 4H-I), while the other phenotypes, *i.e.*, small and surveying ramified, remained stable (Fig. 4J-K; Fig. S5A-E). This suggests that ACI-5891 efficiently forms immune complexes with the extracellular pathological TDP-43 that are eliminated by an Fcγ receptor-mediated mechanism, a hypothesis explored in the next *in vivo* study.

To evaluate whether induction of pTDP-43-removing by phagocytic microglia was associated with substantial alterations in cytokine profiles, several proteins were evaluated in the RIPA-soluble fraction of brain tissue from this study. lL-1β and TNFα levels remained relatively stable ranging from 1 to 2 pg/mL and 2 to 3 pg/mL, respectively, when comparing the vehicle control to ACI-5891 treated mice, while IL-6 and the chemokine, KC/GRO remained within the same range of concentration (Fig. S4H-K).

2.6. ACI-5891 protects neurons from toxicity induced by inoculation of patient brain-derived TDP-43 seeds in mouse brain

Since ACI-5891 potentiated the clearance of TDP-43 neuropathology in the mouse model with the pathology driven by high transgene levels (rNLS8), we further investigated the effect of this mAb in another mouse model with TDP-43 pathology induced by injection of FTLD-TDP patient brain extracts (Porta et al., *2018*). FTLD-TDP extracts were prepared as previously described (Porta et al., 2018), and characterized for the presence of aggregated pTDP-43 and total TDP-43 by immunoblot (Fig. S6A). Their capacity to induce templated aggregation of TDP-43 was confirmed *in vitro* (Fig. S6B).

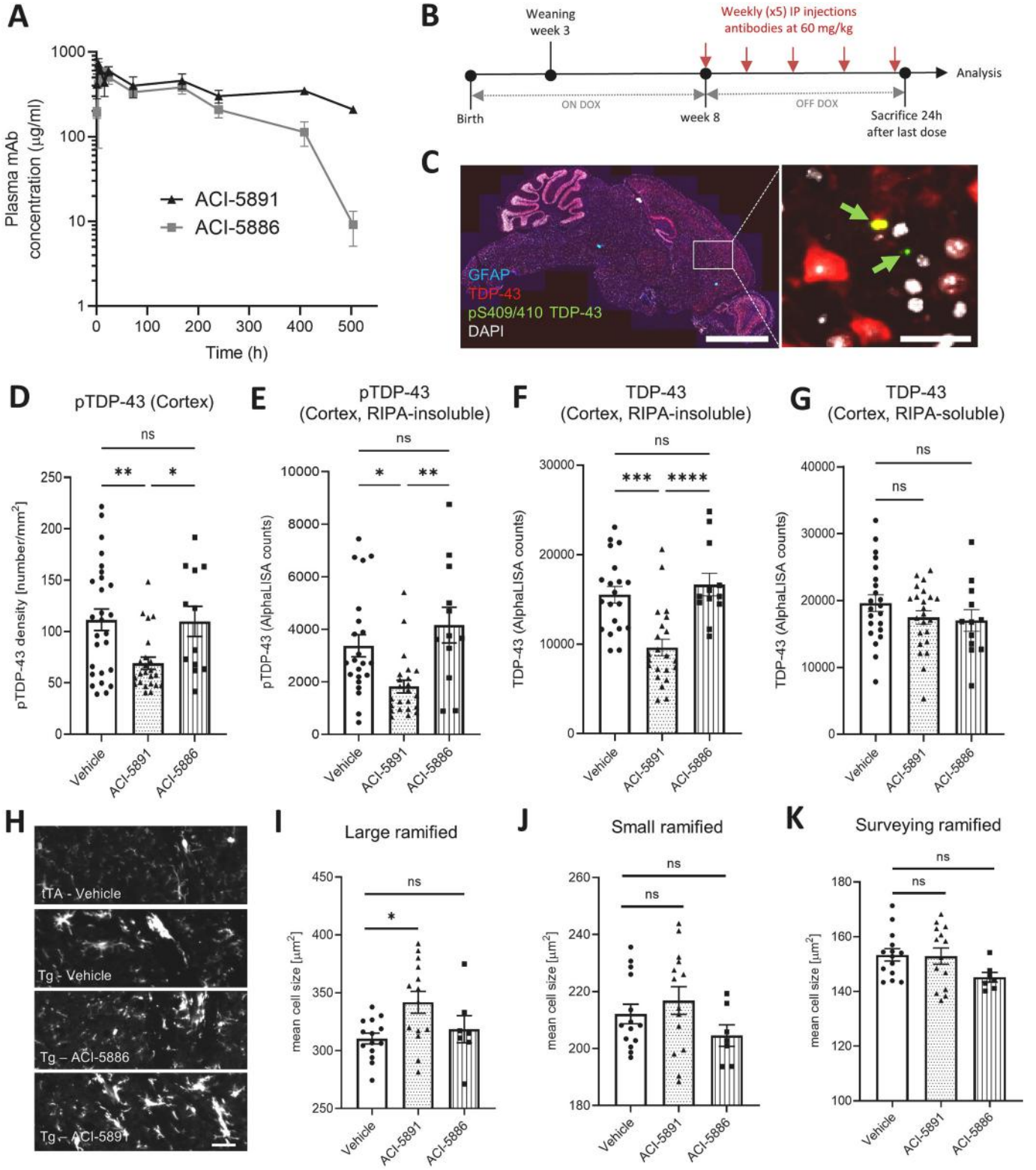

(caption on next page)

Fig. 4. Systemic administration of ACI-5891 reduces neuropathology in rNLS8 mice.
(A) Pharmacokinetic (PK) profiles of ACI-5891 and ACI-5886 after a single-dose intraperitoneal (i.p.) injection in females CD-1 mice. Plasmatic concentrations (y-axis) at various timepoints (x-axis) shown. $N = 3$ mice per group.
(B) Schematic representation of dosing regimen in the *in vivo* study to evaluate the efficacy of TDP-43 antibodies in rNLS8 mice. DOX = doxycycline.
(C) Representative images of pTDP-43 (pS409/pS410) pathology in brain cortex of rNLS8 mice vehicle group. Sections were stained with GFAP (blue), TDP-43 (red), pTDP-43 (green) and DAPI (white). High magnification image of a defined cortical region (white box) is shown with pTDP-43 inclusions indicated by green arrows. Scale bars 2 mm and 50 μm (inset).
(D) pTDP-43 (pS409/pS410) positive object density (number/mm^2) was measured in the cortex of rNLS8 mice treated with vehicle (open bar with solid circles, $n = 27$), ACI-5891 (dotted bar with solid triangles, $n = 23$) or ACI-5886 (striped bar with solid squares, $n = 12$). Each value represents the mean object density of 7 different sections per mouse.
(*E*-G) AlphaLISA counts for pTDP-43 (E) and TDP-43 (F-G) from both RIPA-insoluble (E-F) and RIPA-soluble (G) fractions of rNLS8 mice cortices treated either with vehicle (open bar with solid circles, $n = 20$–22), ACI-5891 (dotted bar with solid triangles, $n = 22$–23) or ACI-5886 (striped bar with solid squares, n = 12).
(H) Representative images of microglial morphology (Iba1 immunostaining) in mouse brain cortex of the 4 groups previously defined. Scale bar = 100 μm.
(I-K) Quantification of mean Iba1 immunoreactive cell size in the cerebral cortex. ACI-5891 (dotted bar, solid triangles) but not ACI-5886 (striped bar, solid squares) treatment significantly increased the size of large ramifying cells compared to vehicle (open bar, solid circles). A one-way ANOVA followed by a Tukey post-hoc test for multiple comparison was used for D-K. *p < 0.05, **$p < 0.01$, ***$p < 0.001$, ****$p < 0.0001$, ns – not significant. Data represent mean ± SEM. (For interpretation of the references to colour in this figure legend, the reader is referred to the web version of this article.)

Following doxycycline removal to induce the transgene expression, CamKIIa-hTDP-43NLSm mice were stereotactically injected with FTLD-TDP brain extracts in the dorsal hippocampus and treated with ACI-5891, ACI-5891 effector-reduced variant (ACI-5891ER) or IgG2a isotype control (Fig. 5A) starting 48 h after inoculation to allow the assessment of therapeutic paradigm. pTDP-43 pathology was detected in hippocampus 3 months post-injection (mpi) (Fig. 5B) with substantial pathology in the ipsilateral side (Fig. S6C). Of note no pTDP-43 was detected at ipsilateral side in non-inoculated mice compared with the inoculated mice (Fig. S6D) consistent with the previous report of rare pTDP-43 inclusions in this mouse model *per se* (Igaz et al., 2011). In the contralateral side pTDP-43 levels were 10 times lower compared to the ipsilateral side, indicative of limited propagation of TDP-43 pathology at 3 mpi (Fig. S6C). Therefore, the effect on neurotoxicity potentiated by pTDP-43 pathology was only evaluated on the ipsilateral side in proximity to the inoculation site in the dentate gyrus (DG). As previously reported, granular neurons in this region of the hippocampus show selective vulnerability (Igaz et al., 2011). Significant neuronal loss (Fig. 5C-D) and the corresponding decrease in DG region size (Fig. S6E) were observed following inoculation of FTLD-TDP brain extracts in the vehicle or isotype control treated mice as compared to non-inoculated mice. Importantly, ACI-5891 significantly reduced neuronal loss in the DG caused by the inoculation of FTLD-TDP brain extracts (Fig. 5D) and showed a trend to preserve the DG region size (Fig. S6E). Interestingly, ACI-5891ER showed a trend towards a rescue of neuronal loss, but its effect was not significant suggesting the requirement of mAb effector function (Fig. 5D, Fig. S6E).

This significant neuroprotection was consistent with a trend to a reduction of density of pTDP-43 inclusions in DG in mice treated with ACI-5891 as compared to the isotype control (Fig. 5E). As in rNLS8 mice, the effects of ACI-5891 were associated with microglial engagement as shown by a trend of increase in Iba1 object density, with significant difference between ACI-5891 and ACI-5891ER variant indicating the requirement of effector function for mAb efficacy (Fig. 5F). Simple linear regression analyses between pTDP-43 and Iba1 object densities showed significance only for mice treated with ACI-5891 ($p = 0.0032$), indicating that ACI-5891-driven neuroprotection was associated with the reduction of pTDP-43 aggregates through activation of microglia (Fig. 5G).

2.7. ACI-5891 potentiates TDP-43 uptake by mouse primary microglia and ALS patient monocyte-derived microglia in vitro

To confirm the direct involvement of microglia in clearing TDP-43 aggregates by Fc-dependent mechanisms, an *in vitro* assay using mouse primary microglia was set up. For this, recombinant TDP-43 aggregates were labeled with pHrodo™ dye which becomes fluorescent upon internalization in an acidic cellular compartment allowing to monitor internalization of TDP-43 aggregates by microglia in real time. Limited internalization of TDP-43 aggregates was observed upon incubation with TDP-43 aggregates alone or in the presence of an isotype control. However, in the presence of ACI-5891, a significant increase in the uptake of labeled TDP-43 aggregates was observed (Fig. 6A) with maximum increase achieved between 5 and 10 h (Fig. 6B). Moreover, mutations in the Fc region of ACI-5891 (ACI-5891ER) resulting in reduced binding to FcγRs, showed a significantly decreased uptake of TDP-43 aggregates as compared with wild-type ACI-5891. Furthermore, ACI-5891 treatment led to a faster clearance of TDP-43 aggregates by microglia as compared to the effector-reduced antibody (Fig. 6B). Moreover, mAb concentration dependent phagocytic uptake was observed with both ACI-5891 and ACI-5891ER, with the latter being consistently lower than ACI-5891 (Fig. S7A). In this assay, ACI-5886 was comparable to ACI-5891 in potentiation of TDP-43 uptake by microglia consistent with its comparable affinity to ACI-5891 for recombinant aggregated TDP-43 (Fig. S7B).

To assess the potential benefits of TDP-43 immunotherapy to patients, the effect of ACI-5891 on uptake of pHrodo-labeled TDP-43 aggregates was evaluated in monocyte-derived microglia (MDMi) from ALS patients. To do so, a chimeric version of ACI-5891 was generated and compared to a human IgG1 isotype control antibody. Monocytes derived from blood of healthy and ALS donors were differentiated into microglia like cells (Fig. 6C). Consistent with mouse primary microglia results, ACI-5891 significantly improved capacity of both ALS and healthy donor's microglia to uptake TDP-43 aggregates as compared with an isotype control antibody (Fig. 6D-E).

3. Discussion

In this study, we demonstrate the relevance of developing a classical immunotherapy approach for altering TDP-43 driven pathology in patients using *in vitro* and *in vivo* models of ALS/FTD. Importantly, our data indicate that the C-terminal epitope is best suited to target the relevant pathological species of human TDP-43. The observed beneficial effects are achieved without perturbing physiological functions of TDP-43 providing a safety rationale for TDP-43 immunotherapy.

As shown by the epitope mapping results, the two mAbs bind to specific epitopes in the RRM (ACI-5886) and the C-terminal region (ACI-5891) of TDP-43. As both mAbs bind with high avidity to TDP-43, it is unlikely that lower monovalent binding affinity of ACI-5886 could explain the differences in functional efficacies observed in this study. Our data demonstrating the utility to specifically target the C-terminal *versus* the RRM domain of TDP-43, aligns with the observations that the C-terminal domain is highly prone to aggregation and is enriched in the pathological inclusions in patient brain homogenates (Arai et al., 2006; Tsuji et al., 2012; Arseni et al., 2021). Importantly, targeting the C-terminal region increases the probability of capturing disease-relevant

C-terminal fragments enriched in patients whereas RRM-binding antibodies may not capture all aggregation-prone fragments especially truncated after amino acid 260 considering the presence of multiple proteolytic sites in this region (Berning and Walker, 2019; Wobst et al., 2017; Yamashita et al., 2012). Moreover, the C-terminal region shown to harbor the amyloid core in pathological TDP-43 aggregates (Arseni et al., 2021; Cao et al., 2019), confers the property of liquid-liquid phase separation (LLPS) (Conicella et al., 2016; Conicella et al., 2020), a physiologic process that allows the functional and dynamic assembly of various membrane-less organelles such as stress granules (Gasset-Rosa et al., 2019). However, under the conditions of chronic stress, irreversible inter- and intra-molecular interactions occur within the C-terminal domain, giving rise to pathologic protein aggregates (Gasset-Rosa et al., 2019). Our mechanistic studies involving recombinant TDP-43 aggregation and cell-based seeding confirm that the efficient capture of TDP-43 seeds prevented templated aggregation. In contrast, when binding the RRM region, inhibition of TDP-43 aggregation and prevention of seeding *in vitro* was significantly lower or absent, suggesting capture of only a fraction of seeding-competent forms of TDP-43.

The two animal models of human disease used in our study were selected to mimic the formation of phosphorylated TDP-43 inclusions, the unique molecular neuropathology hallmark of TDP-43 proteinopathies correlated to the clinical progression of disease (Brettschneider et al., 2013; Kawakami et al., 2019). The differential efficacy of the two mAbs seen *in vitro* translated into reduction of TDP-43 pathology by ACI-5891 but not by ACI-5886 in the rNLS8 mouse model. These data

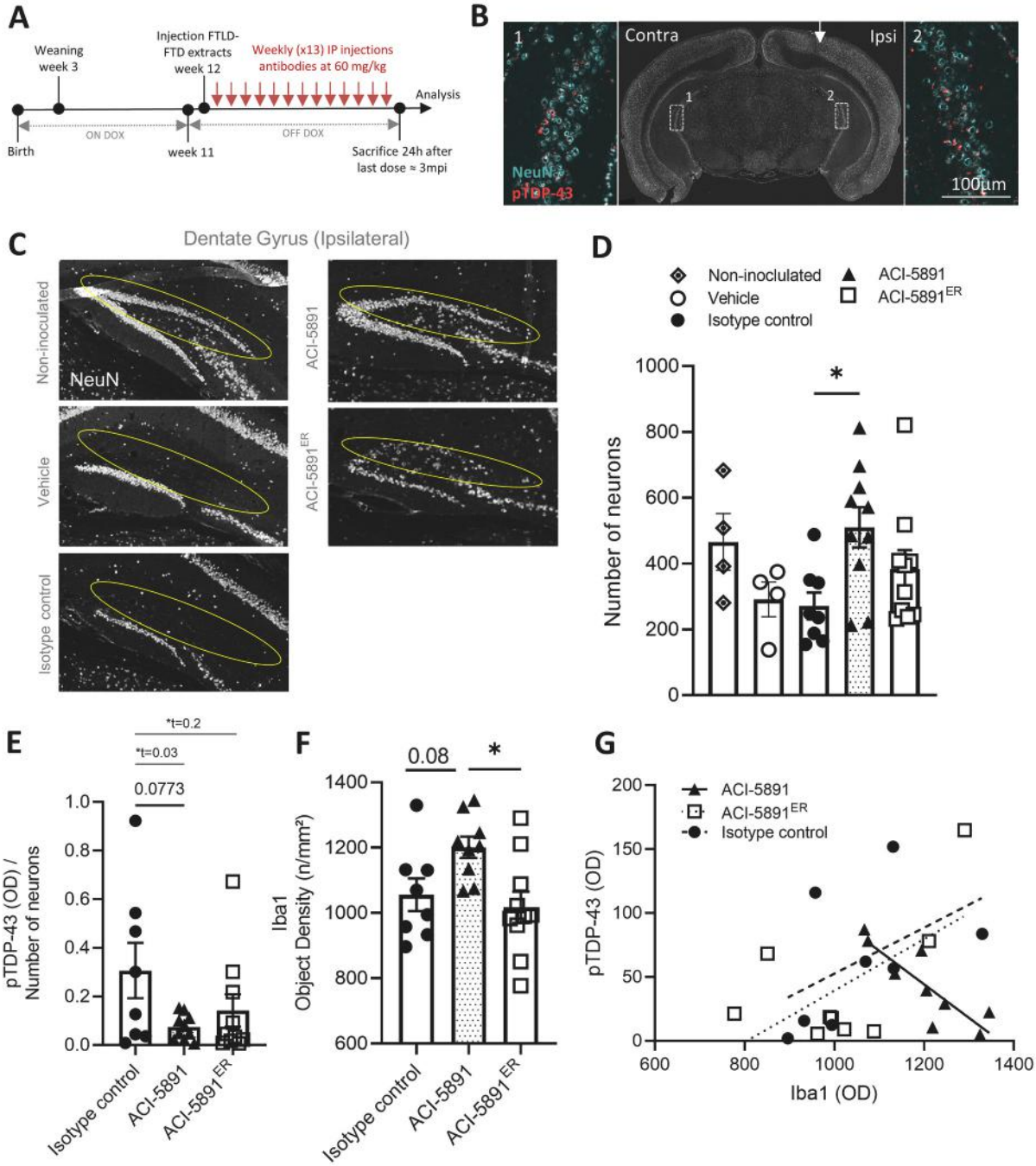

(caption on next page)

Fig. 5. Systemic administration of ACI-5891 confers neuroprotection in CamKIIa-hTDP-43NLSm mice induced by FTLD-TDP brain-derived seeds.
(A) Study design for intrahippocampal inoculation of FTLD-TDP brain extracts and weekly antibody injections in CamKIIa-hTDP-43NLSm mice. Mice were kept on DOX until 11 weeks of age. FTLD-TDP extracts were injected unilaterally in dorsal hippocampus one week after DOX withdrawal, followed by weekly intraperitoneal injection of mAbs for 13 consecutive weeks.
(B) Representative images for NeuN (cyan) and pTDP-43 (red) from mice injected in hippocampus (the white arrow represents the needle track in the ipsilateral side). Scale bar = 100 μm.
(C) Representative images of NeuN immunostaining in the ipsilateral dentate gyrus of non-inoculated and inoculated (FTLD-FTD extracts) mice treated with vehicle, isotype control, ACI-5891 or ACI-5891ER (effector-reduced). Yellow circles indicate the outer shell of the dentate gyrus granular cell layer where neurodegeneration is observed.
(D) Number of NeuN-positive neurons in the ipsilateral dentate gyrus of the mice inoculated with human FTLD-FTD extracts and treated with isotype control ($n = 8$), ACI-5891 ($n = 10$) or ACI-5891ER (n = 10) in addition to non-inoculated ($n = 4$), vehicle (n = 4) groups.
(E) pTDP-43 object density normalized to the number of NeuN-positive neurons in the ipsilateral dentate gyrus of the mice inoculated with human FTLD-FTD extracts and treated with either isotype control, ACI-5891 or ACI-5891ER.
(F) Iba1-positive object density quantified in the ipsilateral dentate gyrus of the same groups previously described.
(G) pTDP-43 object density (y axis) plotted against Iba1 object density (x axis) in the ipsilateral dentate gyrus of the three mice groups (Dashed, solid or dotted lines for isotype control, ACI-5891 and ACI-5891ER groups respectively). Linear regression with trendline is indicated for each group. Pearson correlation: isotype control: $r^2 = 0.2312$, $p = 0.2278$ and y = 0.1799×-127; ACI-5891: $r^2 = 0.7335$, $p = 0.0032$ and y = −0.2621× + 358; ACI-5891ER: $r^2 = 0.3773$, $p = 0.0784$ and y = 0.2015×-162.
The ipsilateral dentate gyrus was used for C-G. A one-way ANOVA followed by a Tukey's post-hoc test for multiple comparison was used for D, E, F. *$p < 0.05$. A Student-*t*-test was performed for indication where *t is indicated. Bars show mean ± SEM. (For interpretation of the references to colour in this figure legend, the reader is referred to the web version of this article.)

demonstrate the relevance of targeting the C-terminal region in clearing extracellular TDP-43. ACI-5891 was able to significantly decrease the levels of aggregated and phosphorylated TDP-43 in the rNLS8 mice, a model with rapidly progressing pathology. Although ACI-5891 binds to both human and mouse TDP-43, its effect on mouse TDP-43 levels could not be evaluated as aggregation of mouse TDP-43 was not observed in this mouse model (Walker et al., 2015). ACI-5886, targeting the RRM domain, was not able to alter pathology. While the RRM domain epitopes proposed in earlier studies (Pozzi et al., 2019; Tamaki et al., 2018) could be useful for intraneuronal targeting, our study led to the identification of a novel epitope for targeting extracellular TDP-43 species for the classical pharmaceutical mAb approach.

The observation of neuroprotective effect of ACI-5891 in the CamKIIa model further demonstrates clinically relevant benefit. The use of these two models allowed us to focus on the evaluation of molecular pathology to better understand the mode of action of our mAbs. However, due to the transgene overexpression, the cognitive and motor phenotypes in rNLS8 mice cannot be overcome by treatments that do not target the transgene expression. No cognitive or motor deficits have been described for CamKIIa mice inoculated with FTLD-TDP brain extracts at 3 mpi, and therefore these readouts were not evaluated.

The observed effect of ACI-5891 can be explained by at least two non-mutually exclusive mechanisms as supported by the *in vitro* and *in vivo* data (Fig. 7). Firstly, as described above, the antibody when bound to the extracellular TDP-43 may prevent TDP-43 templated aggregation by reducing the uptake of seeds by unaffected neurons. Importantly, by using CamKIIa-hTDP-43NLSm inoculated with FTLD-TDP patient brain-derived seeds, our data demonstrated that capture and removal of the extracellular TDP-43 species counteracted the toxic gain-of-function and conferred neuroprotection. Secondly, as demonstrated by our evaluation of microglial activation *in vivo* and *in vitro*, the antibody potentiated the uptake and clearance of extracellular pathological TDP-43 species by microglia thereby preventing the spread of TDP-43 pathology and associated neurotoxicity. ACI-5891 treatment was associated with appearance of hypertrophic microglia indicative of active phagocytosis. Such hypertrophic microglia associated with clearance of TDP-43 pathology have been previously observed in rNLS8 mice during disease recovery induced by turning off the transgene expression (Spiller et al., 2018). Importantly, ACI-5891 treatment did not exacerbate microgliosis. The levels of pro-inflammatory cytokines observed (IL-1beta and TNF-alpha) remain within the limits of assay reproducibility and not of concern as accepted inflammatory danger stimuli such as lipopolysaccharide (LPS) increase levels by at least 5 to 10- fold in mice (Cazareth et al., 2014). Furthermore, ACI-5891 with full effector function demonstrated neuroprotective effect in this study confirming the role of microglial clearance and providing rationale for the need of full effector function for TDP-43 immunotherapy.

Deficient immune function and microglial clearance have been described in aging brain and in neurodegenerative diseases including TDP-43 proteinopathies such as ALS (Malaspina et al., 2015) and FTLD-TDP with progranulin (Wu et al., 2021) and c9orf72 (O'Rourke et al., 2016) mutations. In disease, TDP-43 loss-of-function is suggested to contribute to abnormal microglial activity enhancing synaptic loss (Paolicelli et al., 2017). ALS microglia-like cells derived from monocytes have been shown to display significantly impaired phagocytosis (Quek et al., 2022). Furthermore, the levels of high affinity TDP-43 auto-antibodies decline over time in the patients with ALS which is associated with disease severity (Nielsen et al., 2021). Such a decline may further contribute to impairment of natural mechanisms to clear toxic proteins. Thus, restoration of normal phagocytic pathway through immune complex formation by mAb and Fc-gamma receptor mediated phagocytosis could help to rescue microglial dysfunction. Indeed, ACI-5891 could increase the phagocytic capacity of monocyte-derived microglia from ALS patients.

Thus, ACI-5891 treatment addresses key pathological mechanisms involved in progression of TDP-43 proteinopathies, *i.e.*, extracellular TDP-43 toxicity, seeding and microglial dysfunction, supporting clinical assessment of immunotherapy for the treatment of TDP-43-mediated CNS disorders.

4. Materials and methods

4.1. Vaccine design and preparation

Vaccine was engineered by conjugation of recombinant full-length human TDP-43 (Origene) on the surface of SupraAntigen® liposomes. Monophosphoryl Hexa-acyl Lipid A, 3-Deacyl (Synthetic) (3D-(6-acyl) PHAD®) was used as adjuvant. In addition, adjuvant-free vaccine formulations were manufactured to be used for immune boosts prior to hybridoma fusions from spleenocytes.

4.2. Recombinant antibody production

ACI-5886 and ACI-5891 VH and VL domains were cloned into mammalian expression vectors containing the mouse kappa constant domain and the mouse IgG2a constant domain, respectively. CHO cells were transiently transfected with equimolar of heavy and light chain vectors. Antibodies were purified from supernatants by protein A chromatography (mAb select sure, GE Life sciences) followed by sterile filtration and quantification. Quality control was done by SDS-PAGE,

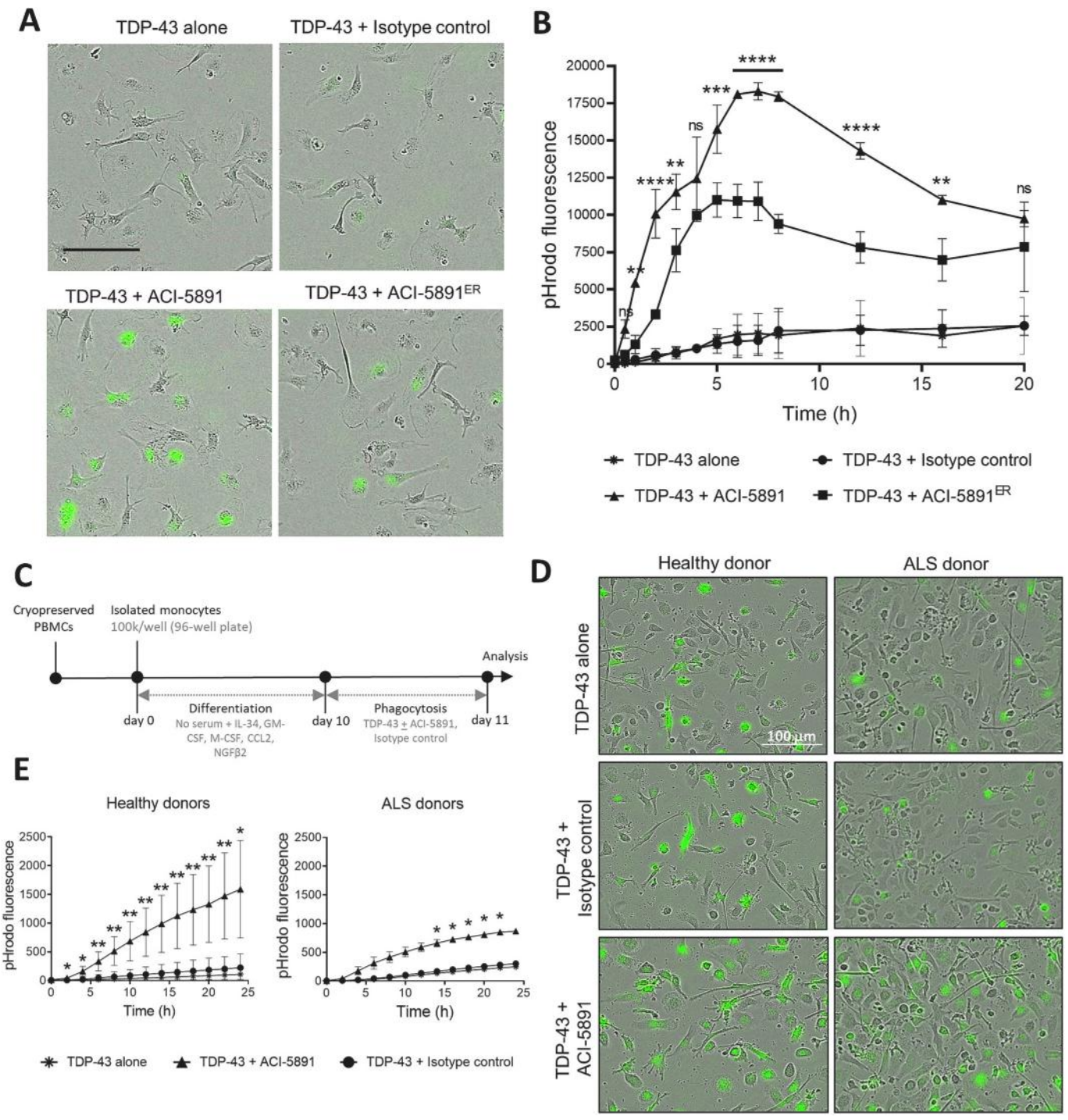

Fig. 6. ACI-5891 promotes phagocytic clearance by microglia *in vitro*.

(A) Representative images of uptake of pHrodo™-labeled recombinant TDP-43 aggregates by mouse primary microglia treated with either isotype control, ACI-5891 or ACI-5891 effector reduced antibody. Scale bar 100 μm.

(B) Integrated intensity of fluorescent pHrodo™ -labeled TDP-43 internalized over time in mouse primary microglia after incubation with ACI-5891 (triangles), ACI-5891 effector-reduced (squares), isotype control (circles) or TDP-43 alone (asterisk). Data represent mean ± SD and are representative of four independent experiments.

(C) Scheme of differentiation of cryopreserved PBMCs from healthy (n = 4) and ALS (n = 2) donors to human monocyte-derived microglia-like cells (MDMi).

(D) Representative images of uptake of pHrodo™-labeled recombinant TDP-43 aggregates by healthy or ALS MDMi cells treated with either isotype control or a chimeric version of ACI-5891.

(E) Integrated intensity of fluorescent pHrodo-labeled TDP-43 internalized over time in MDMi cells after incubation with ACI-5891 (triangles), isotype control (circles) or TDP-43 alone (asterisk). Data represent mean ± SD and are representative of two independent experiments. Scale bar 100 μm.

A two-way ANOVA followed by a Tukey post-hoc test for multiple comparison was used for statistical analysis. Only significance between ACI-5891 and ACI-5891ER for (B) and between ACI-5891 and Isotype control for (E) were reported on the graphs. **p < 0.01, ***p < 0.001, **** p < 0.0001, ns – not significant.

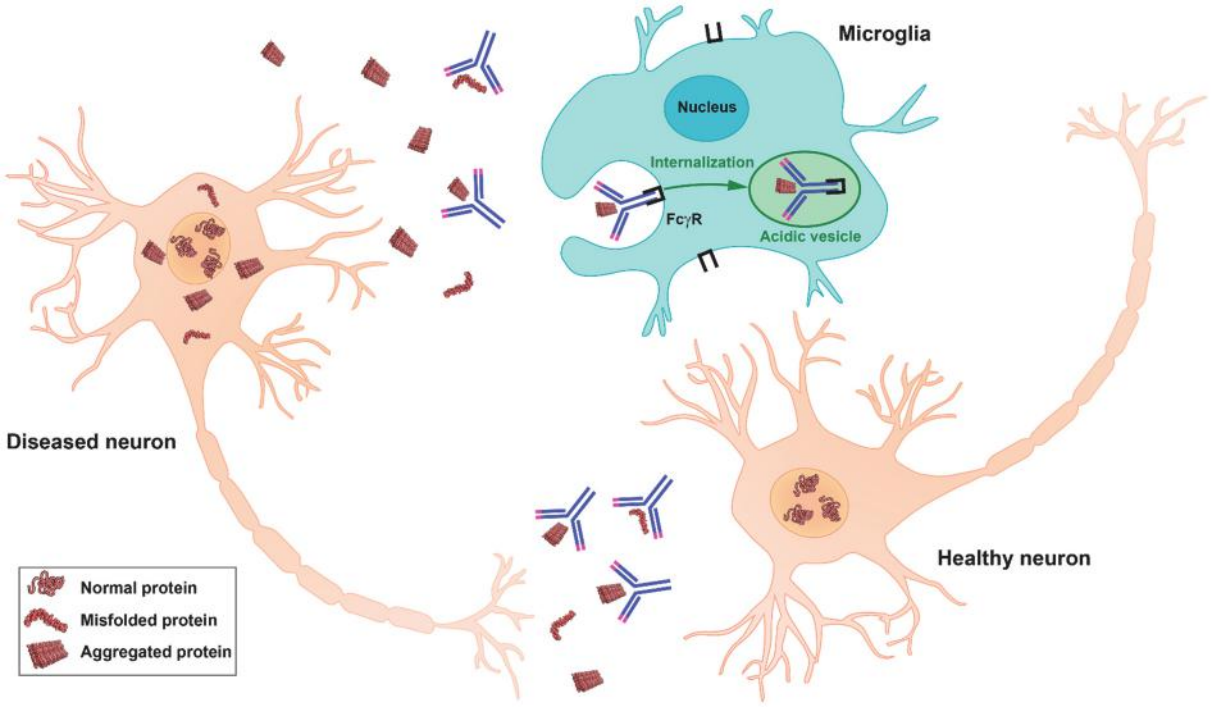

Fig. 7. Proposed mode of action of TDP-43 immunotherapy.
Passive immunotherapy reduces TDP-43 pathology *in vivo* by a combination of various mutually non-exclusive mechanisms. Misfolded TDP-43 released by diseased neurons is captured by antibody in the extracellular space preventing the spread of TDP-43 pathology to a healthy neuron. Moreover, TDP-43 antibody enhances the phagocytic clearance of extracellular misfolded TDP-43 by microglia.

analytical size-exclusion chromatography and endotoxin quantification.

4.3. ELISA

Human recombinant TDP-43 protein was diluted in carbonate-bicarbonate buffer pH 9.6 to a final concentration of 2.5 μg/mL and used to coat ELISA plates (MaxiSorp, Nunc) overnight (ON) at 4 °C, 50 μL/well. After washing four times with PBS / 0.05% Tween®-20 and blocking for one hour at 37 °C with assay buffer (PBS / 0.05% Tween®-20 (Merck 8.22184.0500) / 1% BSA (Sigma: A9418)), plates were incubated for two hours at 37 °C with recombinant ACI-5886 or ACI-5891 diluted to a final starting concentration of 90 ng/mL in PBS / 0.05% Tween-20® / 1% BSA as diluent, followed by seven 3-fold dilutions. Next, plates were washed four times with PBS / 0.05% Tween®-20 and incubated for two hours at 37 °C with goat anti-mouse-AP IgG2a isotype-specific antibody (cat: 115–055-206) at 1:1000 dilution. After washing, plates were incubated for two hours at room temperature (RT) with 1 mg/mL of phosphatase substrate pNPP (S0942, Sigma). The absorbance signal was read at 405 nm wavelength using a plate reader (Tecan Infinity M200).

4.4. Epitope mapping

An initial screening was carried out using a biotinylated (with a linker at the N-terminus) peptide library (Anawa-Biotrend, Switzerland) covering the full sequence of the human TDP-43. The peptides were coated onto streptavidin-coated 96-well plates, and ELISA using ACI-5891 and ACI-5886 were performed as described above. Epitope mapping was also confirmed using a custom-made peptide array library (Pepscan, Netherlands). Briefly, arrays of overlapping linear peptides covering the entire TDP-43 were used (Geysen et al., 1984) to define epitopes.

4.5. Surface plasmon resonance

Avidity measurements were performed on a Biacore T200 instrument (GE Healthcare Life Sciences) using aggregated TDP-43 as ligand bound to the chip surface and recombinantly produced antibodies as analyte in solution.

The instrument was primed with 1× PBS buffer. Flow cells (Fc) 1–4 of a Series S CM5 sensor were activated with a fresh solution of EDC/NHS at 5 μL/min for 420 s. Immediately after activation the ligand injection was performed in respective flow cells. Fc1 was used as a blank. Freshly diluted recombinant human aggregated TDP-43 (Selvita) was injected at 50 μg/mL in 10 mM Na-Acetate buffer pH 4.5 within one minute of preparation at a flow rate of 5 μL/min for 420 s. Next, all channels were quenched with 420 s injection of 1 M Ethanolamine-HCl followed by three regeneration cycles, each injecting 10 mM Glycine pH 1.7 at a flow rate of 5 μL/min for 60 s. Conditions were optimized so that approximately 100 RU protein was immobilized. After baseline stabilization, the run was stopped and buffer was changed from 1×PBS to 1×PBS-P+.

Binding constants of the antibodies were obtained by injecting at the following concentrations from low to high: 0.15, 0.46, 1.37, 4.11, 12.33, 37, 111, and 333 nM in 1x PBS-P^+ at a flow rate of 30 μL/min for 300 s contact time and 600 s dissociation phase. Three regeneration cycles of the ligand surface were performed with 10 mM Glycine-HCl, pH 1.7. A control antibody was run at the beginning and end in every flow channel to control ligand stability. Kinetics were analyzed using a 1:1 fitting model (selecting global fit for Rmax and local RI). Similar kinetic parameters (Ka, Kd and K_D) were also obtained with a 1:1 fitting model obtained by selecting global fit for Rmax and constant RI.

4.6. Recombinant TDP-43 aggregation assay

Human TDP-43 C-terminally fused to maltose binding protein (MBP) separated by a Tobacco Etch Virus (TEV) protease cleavage site was

recombinantly produced in *E. coli*, aliquoted and stored at −80 °C. Storage buffer (20 mM Tris-Cl pH 8.0, 300 mM NaCl, 5% glycerol, 1 mM DTT) was exchanged against assay buffer (30 mM Tris, 150 mM NaCl, pH 7.4) using Centrifugal Filters and the protein concentration was determined by ultraviolet (UV) spectroscopy at 280 nm (NanoDrop). TDP-43-MBP was diluted in assay buffer to a final concentration of 2.5 μM and mixed with 2.5 μM (or serial dilutions as indicated) TDP-43 mAb (ACI-5891, ACI-5886), or isotype control (ACI-5986) in low binding tubes. Aggregation was induced by addition of TEV protease at a final concentration of 10 μg/mL. Aggregation was monitored by absorbance measurement at 600 nm in the center of the well every 15 min with 5 s shaking before each measurement over 24 h in technical triplicates. In order to confirm TEV protease cleavage in the presence of mAbs the samples were analyzed by immunodetection after 1.5 h and the remaining TDP-43-MBP amount was determined. Four μL sample was mixed with 1 μL 5× Mastermix and analyzed in a Separation Module using capillary electrophoresis (Jess, Proteinsimple). ACI-5891 labeled with DyLight680 was used as detection mAb at 20 μg/mL.

For analysis, end points measured by absorbance after 24 h and area under the curve (AUC) over 24 h were normalized to isotype control (ACI-5986) and % aggregated TDP-43 was calculated for each mAb. The results measured by absorbance were confirmed by sedimentation of aggregated TDP-43 and quantification of TDP-43 in supernatant (S) and pellet (P) by immunodetection. Twenty μL of each reaction was centrifuged after 24 h of aggregation at 20,000 ×g for 30 min at 4 °C, supernatant was collected, and the pellet was dissolved in 20 μL PBS by sonication in a water bath. TDP-43 was quantified by immunodetection as described above at 5 s near-infrared (NIR) exposure and expressed as % aggregated TDP-43 in pellet.

4.7. mAb treatment and TDP-43 knock-down using siRNA in C17.2 and HEK-293 cells

One day following the plating, C17.2 and HEK-293 cells were treated with 30 nM of isotype control, ACI-5886 or ACI-5891 for 48 h, prior to RNA or protein analyses. As a positive control for the functional assessment, depletion of the endogenous mouse (C17.2) or human (HEK-293) TDP-43 was done using a specific siRNA (20 nM, (Afroz et al., 2017) transfected with Lipofectamine (Lipofectamine™ 2000 Transfection Reagent) for 48 h, according to manufacturer's instructions and as previously described (Afroz et al., 2017). The mouse and human TDP-43 sequences targeted by this siRNA are 95% identical with one mismatch (out of 21 nucleotides) to the human TDP-43. Therefore, specific downregulation of human TDP-43 was also achieved using the same siRNA sequence, as single mismatches are well tolerated and target sites containing such mismatches are efficiently silenced (Du et al., 2005).

siRNA sequences are provided below:

TDP-43 siRNA 5′-AGGAAUCAGCGUGCAUAUAUU-3.

Control siRNA 5′-GUGCACAUGAGUGAGAUUU-3′.

For protein analysis, total cell lysates were prepared using RIPA buffer (Thermo scientific reference 89,900). Four μL of sample lysates were mixed with 1 μL of 5× Mastermix and analyzed in a separation module using capillary electrophoresis (Jess, Proteinsimple). ACI-5891 labeled with DyLight680 was used as a detection mAb at 20 μg/mL. Consistent with the manufacturer's observations, TDP-43 molecular weight was observed slightly higher than 43 kDa as compared to that seen on the conventional western blots.

4.8. RNA extraction and quantitative reverse transcription (RT)-PCR

Total RNA from C17.2 cells was obtained using RNeasy Plus Mini Kit according to the manufacturer's instructions. Complementary DNA was generated using oligo-dT primers and Maxima H Minus reverse transcriptase (Maxima H minus First Strand cDNA Synthesis kit with dsDNase) as instructed by the manufacturer. Selected TDP-43 splicing targets were tested by RT-PCR amplification using 28 cycles with specific primers (Supplementary Table 3) using Phusion Plus DNA polymerase (Phusion Plus PCR Master Mix). RT-PCR reaction products were analyzed on 10% polyacrylamide gels following staining with SYBR Safe reagent (Invitrogen). Quantification of distinct splice isoforms was done using ImageJ software (US National Institutes of Health). Ratios of intensity between RT-PCR products with exon inclusion and exclusion were averaged for two biological replicates per condition.

4.9. TDP-43 immunodepletion from brain extracts

Sarkosyl-insoluble brain fractions (Sarko-spin) were prepared as in (Laferriere et al., 2019). Immunodepletion was performed using Dynabeads® protein G magnetic beads. For a single reaction, 20 μL of beads were used with 10 μg of antibody for 10 μg of sarkosyl-insoluble brain extracts (total protein). Before addition of antibodies, beads were first rinsed twice with 500 μL PBS-0.05% Tween®-20 and then washed with 100 μL of PBS-0.05% Tween®-20. 100 μL of antibodies at 100 μg/mL in PBS-0.05% Tween®-20 was used to re-suspend the beads. The beads/antibody reaction was incubated for 1 h at room temperature under constant rotation and shaking (HulaMixer™ Sample Mixer 15920D, Thermofisher). The beads/antibody complexes were rinsed twice with PBS-0.05% Tween®-20 and once with PBS before addition of sarkosyl-insoluble brain extracts. The pool of FTLD-TDP type A brain extract was diluted to 100 μg/mL. The beads/antibody complexes were re-suspended using 100 μL of extract and incubated overnight at 4 °C under constant rotation and shaking. Supernatants were collected as immuno-depleted fractions using the magnetic support and kept at −80 °C until characterization by western blotting. Total TDP-43 or the 25 kDa CTF signal on western blot was detected with the C-terminal specific TDP-43 mAb ACI-5891, which has been shown to bind efficiently to both full-length and disease-related C-terminal fragments. The signal of the TDP-43 bands was quantified using ImageJ software (US National Institutes of Health) and normalized to that of the input set at 100%.

4.10. Cell-based TDP-43 templated aggregation assay

Doxycycline inducible iGFP-NLSm cells (Porta et al., 2018) were transduced with the immunodepleted FTLD-TDP sarkosyl-insoluble brain extract pool using Ab-DeliverIN™ (AI21000, OZ Biosciences). Ab-DeliverIN™ (0.5 μL per well of a 96-well plate) was pre-mixed with the immunodepleted extracts and incubated for 15 min at RT. Seventeen microliters of OPTIMEM per well were added onto the mix. Twenty microliters of the reaction were added in each well and incubated for 4.5 h at 37 °C, 5% CO_2 in humidified atmosphere. The media was exchanged for culture media containing 1 μg/mL Doxycycline (DOX).

4.11. In vivo efficacy study in NEFH-hTDP-43NLSm (rNLS8) transgenic mice

Naïve male and female WT and Tg mice were bred at PsychoGenics. NEFH-tTA (JAX 025397) and hTDP-43ΔNLS (JAX 014650) mouse lines were on a hybrid C57BL6C3F1 background strain and obtained from the Jackson Laboratory. Animals were assigned unique identification numbers and housed in OptiMice ventilated racks. Since the historical data from this model was limited, the recommendation described in the guidelines for preclinical animal research in ALS/MND (Ludolph et al., 2010) was applied to inform the group size for the study to evaluate behavior, histology and biochemistry readouts ($n = 15$ for each sex). A total of 96 mixed gender mice were used in this study. Prior to the initiation of the study, all animals were acclimated to the environment, examined, handled, and weighed to ensure adequate health and suitability and to minimize non-specific stress associated with manipulation. Mice were kept on chow which contained DOX (200 mg/kg; Envigo Teklad DOX Diet, Product # TD.08839) during breeding and until the

weaned animals scheduled for testing reached 8 weeks of age, at which point they were placed on regular chow.

Throughout the study, light/dark cycles (12/12), room temperature (20–23 °C) and relative humidity (around 50%), were maintained. Chow and water were provided *ad libitum* for the duration of the study. When mice started to display movement difficulties, they were provided with wet chow and hydrogel on the cage floor. All tests were performed during the animal's light cycle phase and all animal experiments performed at Psychogenics were conducted in compliance with the NIH ethical regulations and standards for animal research and welfare.

ACI-5891 (cross-reactive with human and mouse TDP-43) and ACI-5886 (human-specific) were provided as weekly aliquots and stored in −80 °C freezer. On the day of injection, ACI-5891 (60 mg/kg), ACI-5886 (60 mg/kg) and vehicle were freshly prepared and administered i.p. weekly at a dose volume of 10 mL/kg. The following buffer was used as vehicle: 25 mM Histidine, 200 mM Sucrose, 0.02% Tween®-80, pH 5.5. Dosing began as soon as the antibodies were received. DOX-containing chow was replaced with regular chow at the time of the first injection. Specifically, upon receiving the first injection, the animal was returned to the home cage at which point the DOX-containing chow was replaced with regular chow. Hence, this time point was designated as "0 Weeks off DOX".

4.12. In vivo efficacy study in CamKIIa-hTDP-43NLSm transgenic mice injected with FTLD-TDP brain extracts

Double transgenic CamKIIa-hTDP43NLSm animals were generated by crossing hemizygous females (JAX Stock # 14650: B6;C3-Tg(tetO-TARDBP*)4Vle/J) with hemizygous males (JAX Stock # 007004: B6.Cg-Tg(CamKIIa-tTA)1Mmay/DboJ). Based on power calculations for histological neuropathology evaluation from other models of neurodegeneration, a group size of $n = 8$–10 was predicted. Additionally, to ensure this number for the final analysis and to allow for a 60–70% success rate of stereotactic surgery and inoculation of patient brain extracts, the initial group size was defined as $n = 15$ per treatment group. As no sex-specific differences in the progression of pathology have been described in this model (Porta et al., 2018), this study was conducted in a mixed sex cohort. A total of 52 mixed gender mice were used in this study. Housing conditions were similar as previously described for rNLS8 mice. Breeders and mice were kept on 200 mg/kg DOX diet until 11 weeks of age. At 3 months-old, CamKIIa-hTDP43NLSm mice were deeply anesthetized with isoflurane and immobilized in a stereotaxic frame. Human sarkosyl-insoluble extracts were sonicated prior injection in the dorsal hippocampus. Each injection site (Bregma: antero-posterior: −2.5 mm; lateral: +2 mm; dorso-ventral: −2.4 mm) received 2.5 µl of sarkosyl insoluble human extract at a rate of 0.6 µl/min with a 4 min rest period following injection. One week later, weekly intraperitoneal injection of mAbs (60 mg/kg) started, for 13 consecutive weeks. 3 different antibodies were tested: ACI-5891, ACI-5891 effector-reduced (ACI-5891ER) and isotype control (IgG2a). Terminal collection was done 3 months post injection.

4.13. Human pTDP-43 specific AlphaLISA assay

Immunoassay for detection and quantification of pTDP-43 (pS409/S410) by AlphaLISA technology was developed in-house using an AC Immune's proprietary antibody conjugated with acceptor beads (ref. 6,772,002, Perkin Elmer) and rat pTDP-43 pS409/410 mAb (829,901, BioLegend) biotinylated using the SiteClick™ Biotin Antibody Labeling Kit (ref. S20033, Invitrogen). A 384-well plate (light gray Alphaplate, 6,005,350, Perkin Elmer) was used and the following reagents were added: 5 µL of test samples and 20 µL of acceptor beads at 5 µg/mL and biotinylated antibody at 1.25 nM. After incubation at room temperature for 1 h, 25 µL of Streptavidin donor beads (Perkin Elmer) at 20 µg/mL were added, in the dark. The fluorescence was read after 30 min of incubation using the EnSpire Alpha instrument at 615 nm and EnSpire workstation, version 4.13. The samples were tested in duplicates.

4.14. TDP-43 aggregates uptake by mouse primary microglia

Microglia were plated at 30,000 cells per well in growth medium and incubated for 48 h. Immunocomplexes were prepared in basal medium at 2× final concentration by mixing pHrodoTM labeled TDP-43 aggregates and different antibodies in a dilution plate (Eppendorf 96-well sterile) and incubating O/N at 4 °C. The dilution plate was equilibrated at RT while the cells were washed three times with basal medium. After the final wash, 100 µL of basal medium remained on the cells to which 100 µL of pHrodoTM labeled TDP-43 aggregates from dilution plate was added. Cells were immediately placed inside the Incucyte for live imaging of phase contrast and green fluorescence for 24 h.

4.15. Generation of monocyte-derived microglia-like cells (MDMi)

Peripheral blood mononuclear cells (PBMCs) from healthy and ALS donors were used to derive microglia-like cells from monocytes following the protocol previously described (Ryan et al., 2017). Briefly, isolated monocytes from cryopreserved PBMCs (from 7 healthy and 2 ALS donors) were plated at 100, 000 monocytes per well. Differentiation to MDMi was induced by incubation with IL-34 (100 ng/ml), GM-CSF (10 ng/ml), M-CSF (10 ng/ml), CCL2 (100 ng/ml) and NGFβ2 (10 ng/ml) in an incubator (37 °C; 5% CO_2) for 10 days and without serum. Phagocytosis experiments using pHrodo™ labeled TDP-43 aggregates were done similarly to the mouse primary microglia as described above. The same ACI-5891 antibody was reformatted and produced as human IgG1 chimera and a human IgG1 isotype control was used.

4.16. Statistics

Graphs represent the means of all samples in each group ± SEM or ± SD for *in vivo* and *in vitro* experiments respectively. Sample sizes (n values) and statistical tests are indicated in each figure legend. Normal distribution of the samples was first evaluated using a Shapiro-Wilk test ($\alpha = 0.05$). One-way ANOVA, two-way ANOVA and Student's *t*-test were used as parametric tests followed by a Tukey's test for post-hoc analysis when the ANOVA is significant. A non-parametric Kruskal-Wallis test followed by a Dunn's test for post-hoc analysis was used when the normal distribution of the samples was not validated. Significance (two-tailed) is reported at $^{*}p < 0.05$, $^{**}p < 0.01$, $^{***}p < 0.001$ and $^{****}p < 0.0001$. Outliers in histological measurements were excluded from the graphs and analyses using a Grubb's test with $\alpha = 0.05$ or because of technical reasons (blurred images, folding, disruption or similar based on remarks noted during delineations). For the *in vivo* data shown in Fig. 5E, a trend towards a decrease in pTDP-43 was observed based on a *p*-value of 0.0773 between the isotype control and ACI-5891 treated groups (based on ANOVA followed by a Tukey test). This was further supported by the t-test between these two equally sized groups. Similarly, for the data shown in fig. S6E, even though the difference between isotype control and ACI-5891 treated animals did not reach significance (with one-way ANOVA followed by a Tukey's test), the trend of increase in region size was supported by a t-test between these two groups of equal size.

Supplementary data to this article can be found online at https://doi.org/10.1016/j.nbd.2023.106050.

Funding

This study was funded by AC Immune SA.

Author contributions

T.A., T.S., J.S., M.K., A.P. conceived the study. T.A., T.S., E.C., T.Z., M.A., M.C., M.N., P.N., D.H., C.D., R.M., L.M., M.R., A.B.S., A.B., O.A., S.

P., V.L. and A.P. contributed to the experimental design and interpretation of data and critically revised the manuscript. R.O. contributed to antibody cloning and characterization. A.E., T.Z., M.A., E.C., D.H. contributed to the *in vivo* study data analysis. V.E. performed the immunization studies. K.P. and M.C. contributed to pharmacokinetic assessment. T.A., T.S. and M.K. wrote the manuscript.

Declaration of Competing Interest

T.A., T.S. and T.Z. are coinventors on a patent application, publication number WO2020/234473 entitled "ANTI-TDP-43 BINDING MOLECULES AND USES THEREOF." T.A., T.S., E.C., A.E., L.M. M.A., R.M., R. O., K.P., M.C., C.D., A.B.S., V.E., O.A., A.P. and M.K are employees of AC Immune and entitled to options and/or shares. A.B., J.S. A.E., and T.Z. were employees of AC Immune at the time of this study. M.N., V.L. and S. P. received research funding from AC Immune. The other authors declare no competing interests.

Data availability

All data associated with this study are in the paper or the Supplementary Materials.

Acknowledgements

We thank R. Burai and C. Petite for their help in preparation and characterization of SupraAntigen® vaccine formulation; Y. Kremer for providing the illustration for Fig. 7; C. Alliod for preparation of microglial cultures; M. Gödan and J. Hanselmann for technical support; Psychogenics *in vivo* team and T. Hanania for performing the *in vivo* study. We thank Prof. William Seeley and Neurodegenerative Disease Brain Bank UCSF (funding support from NIH grants P01AG019724 and P50AG023501, the Consortium for Frontotemporal Dementia Research, and the Tau Consortium); Netherlands Brain Bank, Netherlands Institute for Neuroscience, Amsterdam; Prof. Tammaryn Lashley and Queen Square Brain Bank for Neurological Disorders, UCL, and the Brain Bank affiliated with the German Center for Neurodegenerative Diseases (DZNE) and the University Hospital of Tübingen for providing post-mortem human brain and spinal cord tissues. We thank Prof. Clotilde Lagier-Tourenne and Prof. James Berry for providing PBMCs from ALS donors.

References

Afroz, T., Hock, E.M., Ernst, P., Foglieni, C., Jambeau, M., Gilhespy, L.A.B., et al., 2017. Functional and dynamic polymerization of the ALS-linked protein TDP-43 antagonizes its pathologic aggregation. Nat. Commun. 8 (1), 45.

Arai, T., Hasegawa, M., Akiyama, H., Ikeda, K., Nonaka, T., Mori, H., et al., 2006. TDP-43 is a component of ubiquitin-positive tau-negative inclusions in frontotemporal lobar degeneration and amyotrophic lateral sclerosis. Biochem. Biophys. Res. Commun. 351 (3), 602–611.

Arseni, D., Hasegawa, M., Murzin, A.G., Kametani, F., Arai, M., Yoshida, M., et al., 2021. Structure of pathological TDP-43 filaments from ALS with FTLD. Nature 601, 139–143.

Berning, B.A., Walker, A.K., 2019. The pathobiology of TDP-43 C-terminal fragments in ALS and FTLD. Front. Neurosci. 13, 335.

Brettschneider, J., Del Tredici, K., Toledo, J.B., Robinson, J.L., Irwin, D.J., Grossman, M., et al., 2013. Stages of pTDP-43 pathology in amyotrophic lateral sclerosis. Ann. Neurol. 74 (1), 20–38.

Buratti, E., 2018. TDP-43 post-translational modifications in health and disease. Expert Opin. Ther. Targets 22 (3), 279–293.

Cao, Q., Boyer, D.R., Sawaya, M.R., Ge, P., Eisenberg, D.S., 2019. Cryo-EM structures of four polymorphic TDP-43 amyloid cores. Nat. Struct. Mol. Biol. 26 (7), 619–627.

Cazareth, J., Guyon, A., Heurteaux, C., Chabry, J., Petit-Paitel, A., 2014. Molecular and cellular neuroinflammatory status of mouse brain after systemic lipopolysaccharide challenge: importance of CCR2/CCL2 signaling. J. Neuroinflammation 11, 132.

Chornenkyy, Y., Fardo, D.W., Nelson, P.T., 2019. Tau and TDP-43 proteinopathies: kindred pathologic cascades and genetic pleiotropy. Lab. Investig. 99 (7), 993–1007.

Cohen, T.J., Hwang, A.W., Restrepo, C.R., Yuan, C.X., Trojanowski, J.Q., Lee, V.M., 2015. An acetylation switch controls TDP-43 function and aggregation propensity. Nat. Commun. 6, 5845.

Conicella, A.E., Zerze, G.H., Mittal, J., Fawzi, N.L., 2016. ALS mutations disrupt phase separation mediated by alpha-helical structure in the TDP-43 low-complexity C-terminal domain. Structure. 24 (9), 1537–1549.

Conicella, A.E., Dignon, G.L., Zerze, G.H., Schmidt, H.B., D'Ordine, A.M., Kim, Y.C., et al., 2020. TDP-43 alpha-helical structure tunes liquid-liquid phase separation and function. Proc. Natl. Acad. Sci. U. S. A. 117 (11), 5883–5894.

Conti, E., Sala, G., Diamanti, S., Casati, M., Lunetta, C., Gerardi, F., et al., 2021. Serum naturally occurring anti-TDP-43 auto-antibodies are increased in amyotrophic lateral sclerosis. Sci. Rep. 11 (1), 1978.

Du, Q., Thonberg, H., Wang, J., Wahlestedt, C., Liang, Z., 2005. A systematic analysis of the silencing effects of an active siRNA at all single-nucleotide mismatched target sites. Nucleic Acids Res. 33 (5), 1671–1677.

Feiler, M.S., Strobel, B., Freischmidt, A., Helferich, A.M., Kappel, J., Brewer, B.M., et al., 2015. TDP-43 is intercellularly transmitted across axon terminals. J. Cell Biol. 211 (4), 897–911.

Feneberg, E., Gray, E., Ansorge, O., Talbot, K., Turner, M.R., 2018. Towards a TDP-43-based biomarker for ALS and FTLD. Mol. Neurobiol. 55 (10), 7789–7801.

Gasset-Rosa, F., Lu, S., Yu, H., Chen, C., Melamed, Z., Guo, L., et al., 2019. Cytoplasmic TDP-43 De-mixing independent of stress granules drives inhibition of nuclear import, loss of nuclear TDP-43, and cell death. Neuron. 102 (2), 339–57 e7.

Geysen, H.M., Meloen, R.H., Barteling, S.J., 1984. Use of peptide synthesis to probe viral antigens for epitopes to a resolution of a single amino acid. Proc. Natl. Acad. Sci. U. S. A. 81 (13), 3998–4002.

Guenther, E.L., Cao, Q., Trinh, H., Lu, J., Sawaya, M.R., Cascio, D., et al., 2018. Atomic structures of TDP-43 LCD segments and insights into reversible or pathogenic aggregation. Nat. Struct. Mol. Biol. 25 (6), 463–471.

Hergesheimer, R.C., Chami, A.A., de Assis, D.R., Vourc'h, P., Andres, C.R., Corcia, P., et al., 2019. The debated toxic role of aggregated TDP-43 in amyotrophic lateral sclerosis: a resolution in sight? Brain. 142 (5), 1176–1194.

Igaz, L.M., Kwong, L.K., Lee, E.B., Chen-Plotkin, A., Swanson, E., Unger, T., et al., 2011. Dysregulation of the ALS-associated gene TDP-43 leads to neuronal death and degeneration in mice. J. Clin. Invest. 121 (2), 726–738.

Karanth, S., Nelson, P.T., Katsumata, Y., Kryscio, R.J., Schmitt, F.A., Fardo, D.W., et al., 2020. Prevalence and clinical phenotype of quadruple misfolded proteins in older adults. JAMA Neurol.77 (10),, 1299–1307.

Kawakami, I., Arai, T., Hasegawa, M., 2019. The basis of clinicopathological heterogeneity in TDP-43 proteinopathy. Acta Neuropathol. 138 (5), 751–770.

Kouhi, A., Pachipulusu, V., Kapenstein, T., Hu, P., Epstein, A.L., Khawli, L.A., 2021. Brain disposition of antibody-based therapeutics: dogma, approaches and perspectives. Int. J. Mol. Sci. 22 (12).

Laferriere, F., Maniecka, Z., Perez-Berlanga, M., Hruska-Plochan, M., Gilhespy, L., Hock, E.M., et al., 2019. TDP-43 extracted from frontotemporal lobar degeneration subject brains displays distinct aggregate assemblies and neurotoxic effects reflecting disease progression rates. Nat. Neurosci. 22 (1), 65–77.

Lee, E.B., Porta, S., Michael Baer, G., Xu, Y., Suh, E., Kwong, L.K., et al., 2017. Expansion of the classification of FTLD-TDP: distinct pathology associated with rapidly progressive frontotemporal degeneration. Acta Neuropathol. 134 (1), 65–78.

Ludolph, A.C., Bendotti, C., Blaugrund, E., Chio, A., Greensmith, L., Loeffler, J.P., et al., 2010. Guidelines for preclinical animal research in ALS/MND: a consensus meeting. Amyotroph. Lateral Scler. 11 (1–2), 38–45.

Mackenzie, I.R., Neumann, M., Cairns, N.J., Munoz, D.G., Isaacs, A.M., 2011. Novel types of frontotemporal lobar degeneration: beyond tau and TDP-43. J. Mol. Neurosci. 45 (3), 402–408.

Malaspina, A., Puentes, F., Amor, S., 2015. Disease origin and progression in amyotrophic lateral sclerosis: an immunology perspective. Int. Immunol. 27 (3), 117–129.

Maurel, C., Chami, A.A., Thepault, R.A., Marouillat, S., Blasco, H., Corcia, P., et al., 2020. A role for SUMOylation in the formation and cellular localization of TDP-43 aggregates in amyotrophic lateral sclerosis. Mol. Neurobiol. 57 (3), 1361–1373.

McKee, A.C., Gavett, B.E., Stern, R.A., Nowinski, C.J., Cantu, R.C., Kowall, N.W., et al., 2010. TDP-43 proteinopathy and motor neuron disease in chronic traumatic encephalopathy. J. Neuropathol. Exp. Neurol. 69 (9), 918–929.

Muhs, A., Hickman, D.T., Pihlgren, M., Chuard, N., Giriens, V., Meerschman, C., et al., 2007. Liposomal vaccines with conformation-specific amyloid peptide antigens define immune response and efficacy in APP transgenic mice. Proc. Natl. Acad. Sci. U. S. A. 104 (23), 9810–9815.

Nelson, P.T., Dickson, D.W., Trojanowski, J.Q., Jack, C.R., Boyle, P.A., Arfanakis, K., et al., 2019. Limbic-predominant age-related TDP-43 encephalopathy (LATE): consensus working group report. Brain. 142 (6), 1503–1527.

Neumann, M., 2009. Molecular neuropathology of TDP-43 proteinopathies. Int. J. Mol. Sci. 10 (1), 232–246.

Neumann, M., Sampathu, D.M., Kwong, L.K., Truax, A.C., Micsenyi, M.C., Chou, T.T., et al., 2006. Ubiquitinated TDP-43 in frontotemporal lobar degeneration and amyotrophic lateral sclerosis. Science. 314 (5796), 130–133.

Neumann, M., Kwong, L.K., Lee, E.B., Kremmer, E., Flatley, A., Xu, Y., et al., 2009. Phosphorylation of S409/410 of TDP-43 is a consistent feature in all sporadic and familial forms of TDP-43 proteinopathies. Acta Neuropathol. 117 (2), 137–149.

Neumann, M., Lee, E.B., Mackenzie, I.R., 2021. Frontotemporal lobar degeneration TDP-43-immunoreactive pathological subtypes: clinical and mechanistic significance. Adv. Exp. Med. Biol. 1281, 201–217.

Nielsen, A.K., Folke, J., Owczarek, S., Svenstrup, K., Winge, K., Pakkenberg, B., et al., 2021. TDP-43-specific autoantibody decline in patients with amyotrophic lateral sclerosis. Neurol. Neuroimmunol. Neuroinflamm. 8 (2).

Nonaka, T., Masuda-Suzukake, M., Arai, T., Hasegawa, Y., Akatsu, H., Obi, T., et al., 2013. Prion-like properties of pathological TDP-43 aggregates from diseased brains. Cell Rep. 4 (1), 124–134.

O'Rourke, J.G., Bogdanik, L., Yanez, A., Lall, D., Wolf, A.J., Muhammad, A.K., et al., 2016. C9orf72 is required for proper macrophage and microglial function in mice. Science. 351 (6279), 1324–1329.
Paolicelli, R.C., Jawaid, A., Henstridge, C.M., Valeri, A., Merlini, M., Robinson, J.L., et al., 2017. TDP-43 depletion in microglia promotes amyloid clearance but also induces synapse loss. Neuron. 95 (2), 297–308 e6.
Porta, S., Xu, Y., Restrepo, C.R., Kwong, L.K., Zhang, B., Brown, H.J., et al., 2018. Patient-derived frontotemporal lobar degeneration brain extracts induce formation and spreading of TDP-43 pathology in vivo. Nat. Commun. 9 (1), 4220.
Pozzi, S., Thammisetty, S.S., Codron, P., Rahimian, R., Plourde, K.V., Soucy, G., et al., 2019. Virus-mediated delivery of antibody targeting TAR DNA-binding protein-43 mitigates associated neuropathology. J. Clin. Invest. 129 (4), 1581–1595.
Quek, H., Cuni-Lopez, C., Stewart, R., Colletti, T., Notaro, A., Nguyen, T.H., et al., 2022. ALS monocyte-derived microglia-like cells reveal cytoplasmic TDP-43 accumulation, DNA damage, and cell-specific impairment of phagocytosis associated with disease progression. J. Neuroinflammation 19 (1), 58.
Ryan, K.J., White, C.C., Patel, K., Xu, J., Olah, M., Replogle, J.M., et al., 2017. A human microglia-like cellular model for assessing the effects of neurodegenerative disease gene variants. Sci. Transl. Med. 9 (421).
Salajegheh, M., Pinkus, J.L., Taylor, J.P., Amato, A.A., Nazareno, R., Baloh, R.H., et al., 2009. Sarcoplasmic redistribution of nuclear TDP-43 in inclusion body myositis. Muscle Nerve 40 (1), 19–31.
Scialo, C., Tran, T.H., Salzano, G., Novi, G., Caponnetto, C., Chio, A., et al., 2020. TDP-43 real-time quaking induced conversion reaction optimization and detection of seeding activity in CSF of amyotrophic lateral sclerosis and frontotemporal dementia patients. Brain Commun. 2 (2) fcaa142.
Seyfried, N.T., Gozal, Y.M., Dammer, E.B., Xia, Q., Duong, D.M., Cheng, D., et al., 2010. Multiplex SILAC analysis of a cellular TDP-43 proteinopathy model reveals protein inclusions associated with SUMOylation and diverse polyubiquitin chains. Mol. Cell. Proteomics 9 (4), 705–718.
Simula, E.R., Arru, G., Zarbo, I.R., Solla, P., Sechi, L.A., 2021. TDP-43 and HERV-K envelope-specific immunogenic epitopes are recognized in ALS patients. Viruses. 13 (11).
Spiller, K.J., Restrepo, C.R., Khan, T., Dominique, M.A., Fang, T.C., Canter, R.G., et al., 2018. Microglia-mediated recovery from ALS-relevant motor neuron degeneration in a mouse model of TDP-43 proteinopathy. Nat. Neurosci. 21 (3), 329–340.
Tamaki, Y., Shodai, A., Morimura, T., Hikiami, R., Minamiyama, S., Ayaki, T., et al., 2018. Elimination of TDP-43 inclusions linked to amyotrophic lateral sclerosis by a misfolding-specific intrabody with dual proteolytic signals. Sci. Rep. 8 (1), 6030.
Tsuji, H., Arai, T., Kametani, F., Nonaka, T., Yamashita, M., Suzukake, M., et al., 2012. Molecular analysis and biochemical classification of TDP-43 proteinopathy. Brain. 135 (Pt 11), 3380–3391.
Walker, A.K., Spiller, K.J., Ge, G., Zheng, A., Xu, Y., Zhou, M., et al., 2015. Functional recovery in new mouse models of ALS/FTLD after clearance of pathological cytoplasmic TDP-43. Acta Neuropathol. 130 (5), 643–660.
Wang, A., Conicella, A.E., Schmidt, H.B., Martin, E.W., Rhoads, S.N., Reeb, A.N., et al., 2018. A single N-terminal phosphomimic disrupts TDP-43 polymerization, phase separation, and RNA splicing. EMBO J. 37 (5).
Wobst, H.J., Delsing, L., Brandon, N.J., Moss, S.J., 2017. Truncation of the TAR DNA-binding protein 43 is not a prerequisite for cytoplasmic relocalization, and is suppressed by caspase inhibition and by introduction of the A90V sequence variant. PLoS One 12 (5), e0177181.
Wu, Y., Shao, W., Todd, T.W., Tong, J., Yue, M., Koga, S., et al., 2021. Microglial lysosome dysfunction contributes to white matter pathology and TDP-43 proteinopathy in GRN-associated FTD. Cell Rep. 36 (8), 109581.
Yamashita, T., Hideyama, T., Hachiga, K., Teramoto, S., Takano, J., Iwata, N., et al., 2012. A role for calpain-dependent cleavage of TDP-43 in amyotrophic lateral sclerosis pathology. Nat. Commun. 3, 1307.